Research Square

Preprints are preliminary reports that have not undergone peer review.
They should not be considered conclusive, used to inform clinical practice,
or referenced by the media as validated information.

Inflammation-Associated Neuronal and Astrocytic Ensembles in the Dorsal Bed Nucleus of the Stria Terminalis Modulate Peripheral Immune Response via the Brain-Spleen Axis

Xijia Xin
Shandong University
Yaqi Tang
Shandong University
Mengdong Shi
Shandong University
Weikai Han
Shandong University
Xi Xu
Shandong University
Chenyu Zhang
Shandong University
Tongtong Meng
Shandong University
Qingwei Yue
Shandong University
E Liu
Shandong University
Jinhao Sun
sunjinhao@sdu.edu.cn
Shandong University

Research Article

Keywords: Neuroimmunity, The bed nucleus of the stria terminalis, Brain-spleen axis, Astrocytes

Posted Date: July 27th, 2026

DOI: https://doi.org/10.21203/rs.3.rs-10434717/v1

License: This work is licensed under a Creative Commons Attribution 4.0 International License.
Read Full License

Additional Declarations: No competing interests reported.

Title

Inflammation-Associated Neuronal and Astrocytic Ensembles in the Dorsal Bed Nucleus of the Stria Terminalis Modulate Peripheral Immune Response via the Brain-Spleen Axis

Xijia Xin[1], Yaqi Tang[1], Mengdong Shi[1], Weikai Han[1], Xi Xu[1], Chenyu Zhang[1], Tongtong Meng[1], Qingwei Yue[1], E Liu[1*], Jinhao Sun[1*]

[1]Department of Anatomy and Neurobiology, Shandong Key Laboratory of Mental Disorders, School of Basic Medical Science, Shandong University, Jinan 250012, Shandong, China

[*]These authors contributed equally to this work.

[*]Correspondence:

Jinhao Sun, Department of Anatomy and Neurobiology, Shandong Key Laboratory of Mental Disorders, School of Basic Medical Science, Shandong University, Jinan 250012, Shandong, China, E-mail: sunjinhao@sdu.edu.cn

E Liu, Department of Anatomy and Neurobiology, Shandong Key Laboratory of Mental Disorders, School of Basic Medical Science, Shandong University, Jinan 250012, Shandong, China, E-mail: liue@sdu.edu.cn

Abstract

The brain detects peripheral inflammatory signals and modulates immune responses, yet the forebrain mechanisms that participate in this process remain

incompletely understood. Here, we identify the dorsal bed nucleus of the stria terminalis (dBNST), a forebrain node that receives convergent inputs from emotion-related brain regions and projects to the dorsal vagal complex (DVC), as a critical hub for peripheral immune regulation. Using chemogenetic and optogenetic approaches, we show that lipopolysaccharide(LPS)-activated Fos^{+} engram neurons in the dBNST are required for immune dysregulation, and that inhibition of these neurons attenuates peripheral immune response. Neural tracing combined with optogenetic functional validation reveals a dBNST-DVC-spleen pathway through which Fos^{dBNST} neurons regulate splenic nerve activity and peripheral immune-cell distribution. We further show that LPS recruits a subpopulation of dBNST astrocytes, selective reactivation of these astrocytes enhances dBNST neuronal excitability and drives peripheral immune alterations. Notably, the injection of LPS elevates adenosine triphosphate (ATP) levels around dBNST astrocytes, which activates $P2Y_1$ receptors and promotes glutamate release, thereby increasing local neuronal excitability. Because astrocytes can integrate signals from multiple neurons and local inflammatory cues, they may function as signal-integrating hubs in brain-immune crosstalk. Together, our findings reveal a coordinated neuron-astrocyte mechanism in the dBNST that encodes immune information, establish astrocytes as key nodes in forebrain regulation of peripheral immunity, and provide a new framework for understanding brain-immune interactions.

Keywords: Neuroimmunity, The bed nucleus of the stria terminalis, Brain-spleen axis, Astrocytes,

1.Introduction

Peripheral immune responses must be strong enough to eliminate pathogens and repair tissue damage, yet sufficiently constrained to prevent excessive inflammation. The spleen is a major peripheral hub for immune homeostasis[1], and accumulating evidence indicates that splenic immune function is under neural control through the brain-spleen axis. For example, optogenetic stimulation of corticotropin-releasing hormone (CRH) neurons in the paraventricular nucleus of the hypothalamus (PVN) or the central amygdala (CeA) increases splenic nerve firing and alters splenic plasma-cell formation, indicating functional neural communication between these stress-related brain regions and the spleen[2]. Similarly, activation of neurons in the dorsal motor nucleus of the vagus nerve (DMV) increases splenic nerve activity, further supporting a role for autonomic brainstem nuclei in brain-spleen crosstalk[3]. Despite these advances, current neuroimmune studies have largely emphasized midbrain and brainstem regions[4-6]. Forebrain contributions remain much less well defined, although recent evidence shows that activation of motor cortical neurons can redistribute systemic immune cells[7]. Thus, identifying forebrain nodes that sense inflammatory signals and transmit regulatory output to peripheral immune organs is an important question.

BNST is one such candidate. It is a forebrain-midbrain interface with complex subregional organization and stress-integrative functions[8, 9]. Under immune challenge conditions, the BNST receives convergent afferent inputs from multiple

upstream brain regions, suggesting that it serves as an important relay and integration hub in the transmission of inflammatory signals to neuroendocrine centers[10]. The importance of the BNST in inflammation regulation has been established. In LPS-induced inflammation models, the BNST has been shown to regulate sleep-weak behavior[11], feeding behavior[12] and anxiety-like behavior[13]. Moreover, activation of BNST neurons is sufficient to sense peripheral interleukin-1β (IL-1β) signals and trigger a series of autonomic and immune responses including tachycardia, reduced core body temperature, and elevated serum Interleukin-6 (IL-6) levels[14]. In an amphetamine self-administration model, the BNST is also involved in regulating anxiety-like behavior, accompanied by changes inlocal inflammatory cytokine expression[15].The dorsal BNST (dBNST) is particularly relevant because it integrates negative emotion-related information and contributes to anxiety and fear regulation[16, 17]. Stress signals can propagate from the central nervous system to peripheral immune organs and substantially reshape immune function[18, 19]. Consistent with this idea, stress exposure alters splenic morphology, function, and immune-cell composition[20, 21], indicating a close relationship between stress-related neural circuits and splenic immune status. Anatomically, retrograde trans-synaptic tracing from the mouse spleen labels neurons in the BNST, suggesting direct or indirect neural connectivity between the BNST and the spleen[22]. Studies have shown that the BNST-PVN neural circuit can regulate mechanical withdrawal threshold and macrophage infiltration in the dorsal root ganglia in a neuropathic pain model via the brain-spleen axis, highlighting the key

regulatory role of the BNST in this axis[23]. Given the established importance of the BNST in inflammation regulation, and the unique position of the dBNST in integrating emotional and autonomic signals that makes it an ideal candidate node for forebrain regulation of the brain-spleen axis, the dBNST may represent a forebrain node through which emotional states and inflammatory signals influence splenic immunity. However, the specific cell types and circuit mechanisms through which the dBNST contributes to this process remain largely undefined.

A second conceptual gap concerns how inflammatory experiences are represented in the brain. In memory research, neuronal ensembles recruited during learning are required and sufficient for later memory retrieval, forming the cellular substrate of memory engrams[24, 25]. This framework has recently been extended to neuroimmunology, where specific neuronal ensembles appear to encode prior inflammatory states. In the insular cortex, inflammation-related engram neurons modulate dextran sulfate sodium (DSS)-induced colitis[26]. In a gastritis model, repeated optogenetic reactivation of PVN neurons that encode inflammatory information recapitulates gastric inflammation and induces inflammatory sensitization without increasing systemic cytokine levels[27]. These studies suggest that immune information can be stored by discrete neuronal ensembles and later retrieved to influence peripheral organs. While the BNST has been shown to harbor inflammation-associated engram neurons, whether these dBNST-specific ensembles regulate peripheral immune response through the brain-spleen axis, remains unknown.

Neuronal engrams, however, are unlikely to operate in isolation. Astrocytes are the most abundant glial cell type in the central nervous system, accounting for approximately 20%-40% of all brain cells [28]. They form intimate associations with neurons and actively regulate neural circuit function[29, 30]. Astrocytes in the lateral habenula could regulate calcium activity in neighboring neurons by releasing gliotransmitters such as glutamate[31]. More recently, learning-associated astrocyte ensembles were shown to respond to memory-inducing stimuli and to generate persistent cellular responses required for memory storage and retrieval[32]. These findings raise the possibility that astrocyte ensembles may also be recruited during immune challenge and may cooperate with local neurons to encode immune-related information. Mechanistically, inflammatory stimuli can elevate brain ATP levels[33], and activation of astrocytic $P2Y_1$ receptors promotes glutamate release. Whether dBNST astrocytes use ATP-$P2Y_1$-glutamate signaling to regulate inflammation-associated neuronal activity and thereby influence peripheral immunity remains unknown[34, 35].

Here, we tested the hypothesis that immune challenge recruits distinct but coexisting Fos^+ neuronal and astrocytic ensembles in the dBNST, and that these cell populations regulate peripheral immune response through the brain-spleen axis. Using activity-dependent labeling, chemogenetic and optogenetic manipulation, retrograde tracing, fiber photometry, and peripheral immune profiling, we examined how dBNST neurons and astrocytes are activated by LPS, how they communicate locally, and how

127 they control splenic nerve activity and immune-cell distribution. This approach allowed
128 us to define a forebrain neuron-astrocyte mechanism for immune information encoding
129 and to identify a dBNST-DVC-spleen circuit through which the forebrain modulates
130 peripheral innate immunity.

131 **2.Abbreviations**

Abbreviation	Full name
4-OHT	4-hydroxytestosterone
ACSF	Artificial cerebrospinal fluid
Arc	Arcuate hypothalamic nucleus
ATP	Adenosine triphosphate
ATPγS	Adenosine 5'-O-(3-thiotriphosphate)
AUC	Area under the curve
CeA	The central amygdala
ChAT	Choline acetyltransferase
CNO	Clozapine N-oxide
CRH	Corticotropin-releasing hormone
dBNST	The dorsal bed nucleus of the stria terminalis
DMV	The dorsal motor nucleus of the vagus nerve
DOX	Doxycycline
DREADD	Designer receptors exclusively activated by designer drugs
DSS	Dextran sulfate sodium

DVC	The dorsal vagal complex
IL-1	Interleukin-1
IL-10	Interleukin-10
IL-17A	Interleukin-17A
IL-1β	Interleukin-1β
IL-6	Interleikin-6
INF-γ	Interferon-gamma
IP3	Inositol 1,4,5-trisphosphate
LC	Locus coeruleus
LPS	Lipopolysaccharide
OCT	Optimal cutting temperature compound
PAG	Periaqueductal gray
PB	Parabrachial nucleus
PBS	Phosphate-buffered saline
PCRtA	Parvicellular reticular formation-alpha
PLC	Phospholipase
PSTh	Parasubthalamic nucleus
PVN	The paraventricular nucleus of the hupothalamus
TNF-α	Tumor necrosis factor-α
TRE	Tetracycline-responsire element

3.Materials and methods

Animals

All animal procedures were reviewed and approved by the Institutional Animal Care and Use Committee of Shandong University. Male mice older than 8 weeks were used in all experiments. Mice had ad libitum access to food and water and were maintained in a temperature-controlled facility under a 12-h light/12-h dark cycle (lights on, 7:00 a.m.-7:00 p.m.), with ambient temperature maintained at 21-25°C and relative humidity at 30%-75%. C57BL/6J mice were obtained from the Department of Laboratory Animal Sciences, Shandong University (Jinan, China). Fos-CreER^{T2} mice (Jackson Laboratory, stock no. 030323) were used in this study. To generate Fos-CreER^{T2} x Rosa-TdT mice for neuronal labeling, Fos-CreER^{T2} mice were crossed with Rosa-TdTomato reporter mice (Jackson Laboratory, stock no. 007914).

Intraperitoneal injection

Escherichia coli-derived LPS (O111:B4; Sigma-Aldrich, L2630) was reconstituted in sterile saline to a stock concentration of 1 mg/mL, aliquoted into single-use volumes, and stored at -20°C until use to avoid repeated freeze-thaw cycles. Before each experiment, one aliquot of the stock was thawed on ice and diluted with sterile saline to an appropriate concentration such that the amount of LPS in the intraperitoneal injection volume per pouse was equivalent to 50μg/kg. As the primary modeling approach in this study, mice received a single intraperitoneal injection of LPS, and tissues were collected 3 h after administration.

For cytokine-administration experiments, mice were randomly assigned to two groups: vehicle-treated controls and the IL-1β+tumor necrosis factor-α (TNF-α) co-administration group. Mice in the cytokine group received an intraperitoneal injection of a mixed solution containing IL-1β (MedChemExpress, USA) at 200 μg/kg and TNF-α (MedChemExpress, USA) at 100 μg/kg. Vehicle-treated controls received an equivalent volume of sterile saline through the same intraperitoneal route.

Flow cytometry

For flow cytometry, single-cell suspensions were prepared in phosphate-buffered saline (PBS) and pre-incubated with Fc Block anti-mouse CD16/CD32 (1:100; BioLegend, #156603) for 15 min to reduce nonspecific Fc receptor binding. Cell viability was assessed using the Zombie Aqua Fixable Viability Kit (1:100; BioLegend, #423101) for 20 min in the dark. After viability staining, fluorochrome-conjugated monoclonal antibodies against surface antigens were added at a dilution of 1:100 and incubated at 4°C for 45 min in the dark. The following antibodies were used for mouse spleen and peripheral blood cells: Alexa Fluor 700 anti-mouse CD45.2 (BioLegend, #109821), FITC anti-mouse CD3 (BioLegend, #100203), PE-Cyanine5.5 anti-mouse CD19 (BioLegend, #152405), FITC anti-mouse F4/80 (BioLegend, #123107), APC anti-mouse CD11b (BioLegend, #101211), PE anti-mouse Ly-6C (BioLegend, #128007), and Brilliant Violet 421 anti-mouse Ly-6G (BioLegend, #127628). After staining, cells were washed twice with PBS and immediately analyzed on a CytoFLEX

flow cytometer (Beckman Coulter, USA). Data were collected and analyzed using CytExpert software (version 2.4).

Immunofluorescence staining

Mice were deeply anesthetized with 1.25% tribromoethanol (0.2 mL per 10 g body weight) and fixed in a fume hood by transcardial perfusion. The thoracic cavity was opened to expose the heart, a perfusion needle was inserted through the cardiac apex, and the right atrium was incised. Animals were perfused with 0.01 M PBS until the effluent became clear, followed by approximately 100 mL of 4% paraformaldehyde for fixation. Brains were harvested, post-fixed in 4% paraformaldehyde at 4°C for 12 h, and dehydrated in 30% sucrose until the tissue sank. Target brain regions were trimmed, embedded in Optimal Cutting Temperature Compound (OCT), and cryopreserved at -80°C. Coronal sections were prepared using a freezing microtome (Leica CM1860, Germany) pre-cooled to -20°C. After initial trimming at 100 μm until the target region was approached, formal sections were cut at 30 μm. Sections were transferred to culture plates containing 0.01 M PBS and stored at 4°C for short-term use or in brain-section antifreeze solution at -20°C for long-term storage.

For immunofluorescence staining, brain sections were transferred to 24-well plates. Antigen retrieval was performed by adding 200 μL of H2O2 retrieval buffer per well and incubating at room temperature for 25 min, followed by three washes with 0.1 M PBS for 5 min each. Trypsin-based retrieval buffer (200 μL per well) was then added and incubated at 37°C for 5 min, followed by three additional washes with 0.1 M PBS.

Sections were blocked with 0.3% Triton X-100 (Solarbio, #T8200) and 5% BSA (Solarbio, #A8020) for 1 h at room temperature. Primary antibodies were diluted with 0.001% trypsin inhibitor and included rabbit anti-c-Fos (1:1000, ab214672, Abcam), guinea pig anti-c-Fos (1:1000, 226308, Synaptic Systems), rabbit anti-ChAT (1:1000, ab181023, Abcam), rabbit anti-Sox9 (1:200, HY-P80335, MedChemExpress), rabbit anti-GFAP (1:1000, GB11096-50, Servicebio), and mouse anti-NeuN (1:1000, E4M5P, Cell Signaling). Sections were incubated with 200 μL of primary antibody solution for 1 h at room temperature and then overnight at 4°C. After three washes with 0.01 M PBS, sections were incubated for 2 h at room temperature in the dark with secondary antibodies: anti-rabbit 488 (1:200, RGAR002, Proteintech), anti-rabbit 594 (1:200, RGAR004, Proteintech), anti-rabbit 647 (1:200, RGAR005, Proteintech), anti-mouse 405 (1:500, AS055, ABclonal), and anti-guinea pig 488 (1:200, Abcam). After three final washes with 0.01 M PBS, sections were mounted on glass slides with DAPI-containing anti-fade mounting medium. Images were acquired using an LSM880 confocal microscope (Zeiss, Germany) and an Olympus confocal microscope (Olympus, Tokyo, Japan). A 20x oil-immersion objective was used when needed for target-region imaging, and images were analyzed using ImageJ software (version 2.14.0).

Measurement of cytokines

To assess cytokine responses after LPS stimulation, wild-type C57BL/6J mice were randomized into experimental groups, including LPS-treated and saline-treated

groups, chemogenetic activation or inhibition groups, optogenetic activation or inhibition groups, astrocyte activation groups, and their corresponding controls. LPS was administered intraperitoneally, and control mice received equivalent volumes of sterile saline through the same route. Peripheral blood was collected from the orbital venous plexus 3 h after stimulation to assess acute cytokine production. Blood samples were allowed to clot at room temperature for 2 h and were then centrifuged at 2,000 x g for 20 min at 4°C to separate serum. Serum was carefully collected, aliquoted into sterile microcentrifuge tubes, and stored at -80°C until analysis. Serum IL-1β and TNF-α levels were quantified using commercially available enzyme-linked immunosorbent assay (ELISA) kits (Wuhan Cloud-Clone) according to the manufacturer's instructions.

Recording of splenic-nerve activity

For splenic nerve activity recording, mice were deeply anesthetized with 1.25% tribromoethanol (0.2 mL/10 g body weight), placed in the supine position, and maintained on a temperature-controlled heating pad at 36.5-37.5°C throughout surgery and recording. The anterior abdominal wall was shaved and disinfected sequentially with 75% ethanol and iodine antiseptic solution. A 1.5-2 cm midline laparotomy was performed to access the abdominal cavity. The spleen was gently exteriorized and kept hydrated with sterile saline. Connective tissue surrounding the splenic nerves was carefully dissected under a stereomicroscope using fine forceps and polished glass needles to avoid nerve damage. A tungsten microelectrode was hooked onto the isolated splenic nerve fibers and connected to a multichannel acquisition and analysis system

(ADInstruments, Australia) for neural signal recording. Signals were processed using LabChart 8 software (ADInstruments, Australia) and digitally filtered at 10-60 Hz to reduce background noise while preserving splenic nerve firing signals.

Stereotaxic surgery and virus injection

All stereotaxic surgeries were performed under aseptic conditions. Mice were deeply anesthetized with 1.25% tribromoethanol (0.2 mL per 10 g body weight) and mounted on a stereotaxic frame (RWD, China) equipped with a temperature-controlled warming platform. After disinfection with 75% ethanol, cranial fur was trimmed, the scalp was disinfected with iodophor, and a midline sagittal incision was made to expose the skull and bregma. The head was secured by placing the incisors in the dental groove and inserting bilateral ear bars into the ear canals. The skull was leveled by aligning the head midline with the stereotaxic nose clamp and ensuring that the skull surface was horizontal. The exposed area was re-disinfected with povidone-iodine before drilling.

Bregma was identified as the origin, and lambda was used to verify skull alignment. Stereotaxic coordinates were determined according to The Mouse Brain Atlas in Stereotaxic Coordinates (Paxinos and Franklin, 2nd edition). A small cranial opening was made at the calibrated injection site with an electric drill, taking care not to damage the dura. For viral injection, 200 nL of virus solution was loaded into a Hamilton syringe, which was slowly lowered to the target depth. Virus was infused at 0.04 μL/min. After infusion, the syringe was left in place for 10 min to allow diffusion and then slowly withdrawn to minimize reflux. The scalp was sutured, and iodophor was

applied for postoperative antisepsis. Mice were placed on a warming pad until fully conscious and monitored for 48 h after surgery. For optogenetic experiments, a guide cannula was positioned 200 μm above the viral injection site and fixed to the skull with self-curing dental acrylic. Maximal AAV expression was typically observed 2-3 weeks after injection, at which time mice were used for subsequent experiments.

Red retrobeads were purchased from Lumafluor. rAAV-F-RAM-d2tTA-hM4Di-EGFP, rAAV-F-RAM-d2tTA-hM3Dq-mCherry, rAAV-F-RAM-d2tTA-mCherry, AAV-hSyn-GCaMP6s, AAV-DIO-eNpHR-GFP, AAV-DIO-ChR2-GFP, AAV-cFos-CreER^{T2}, PRV-CAG-3Gc, AAV-GfaABC1D-DIO-hM3Dq-mCherry, AAV-GfaABC1D-DIO-mCherry, rAAV-GfaABC1D-ATP1.0-L, and rAAV-GfaABC1D-iGluSnFR3.v857.GPI were purchased from Brain Case Co., Ltd. (Wuhan, China). All viruses were stored at -80°C before use, and titers exceeded 10^12 viral particles per milliliter.

Chemogenetic inhibition/activation of Fos^{dBNST} neurons

For chemogenetic manipulation of Fos^{+} neurons in the dBNST, C57BL/6J mice received bilateral stereotaxic injections of rAAV-F-RAM-d2tTA-hM4Di-EGFP, rAAV-F-RAM-d2tTA-hM3Dq-mCherry, or their corresponding control viruses, with a volume of 200 nL per side at coordinates AP +0.14 mm, ML ±0.85 mm, DV -4.3 mm (Braincase). The F-RAM system employs a tetracycline-responsive element (TRE) to regulate Designer Receptors Exclusively Activated by Designer Drugs (DREADD)

expression, with mCherry or EGFP fluorescent reporters for visualization of transduced neurons.

All mice were given ad libitum access to doxycycline (DOX)-supplemented chow (40 mg/kg) starting 24 h prior to viral injection, and this diet was maintained for 3 weeks post-injection to suppress basal viral transgene expression. To specifically label inflammation-activated Fos^+ neurons, DOX chow was withdrawn 24 h prior to LPS administration. Immediately after LPS injection, mice were switched to a high-DOX diet (1000 mg/kg) for 24 h to rapidly terminate the neuronal labeling window, ensuring temporal precision of Fos^+ neuron tagging. Thereafter, the dietary DOX concentration was returned to 40 mg/kg. For inhibition experiments, Clozapine N-oxide (CNO) (3 mg/kg) was administered intraperitoneally 1 h prior to LPS injection, and tissues were collected 3 h after LPS administration. For activation experiments, CNO (3 mg/kg) was administered intraperitoneally to activate hM3Dq-expressing neurons, and spleen, brain, and blood samples were harvested 3 h after CNO administration for subsequent analyses.

Optogenetic inhibition/activation of Fos^{dBNST} neurons

For optogenetic manipulation of Fos^+ neurons in the dBNST, C57BL/6J mice received unilateral stereotaxic injections of a 1:1 mixture of Fos-$CreER^{T2}$ and either AAV-DIO-ChR2-GFP or AAV-DIO-eNpHR-GFP, with a total volume of 400 nL (Braincase). Optical fibers were implanted either ipsilaterally at the injection site or ipsilaterally in the DVC region, and secured to the skull with dental cement.

Three weeks after viral injection, mice received intraperitoneal LPS to induce inflammation, immediately followed by intraperitoneal 4-Hydroxytestosterone (4-OHT) to label LPS-activated Fos^{dBNST} neurons. After a 14-day recovery period, optogenetic stimulation was delivered using a laser system (THINKERTECH, China). For activation experiments, blue light (470 nm, 30 Hz) was delivered for 15 min, and tissues were collected 3 h later. For inhibition experiments, a second LPS injection was administered to re-induce inflammation, together with yellow light stimulation (589 nm, 30 Hz) delivered using a cyclic protocol (10 min on/20 min off) continuously for 3 h. Spleen, brain, and blood samples were collected immediately after stimulation.

Vagotomy

Bilateral subdiaphragmatic vagotomy was performed under aseptic conditions. Mice were anesthetized by intraperitoneal injection of 1.25% tribromoethanol at a dose of 0.2 mL per 10 g body weight. A roughly 1 cm skin incision was made parallel to the midline in the upper abdomen. The liver and stomach were gently retracted to expose the distal esophagus and the two vagal trunks coursing along it. After the nerve trunks were carefully separated from the surrounding connective tissue, a segment approximately 5 mm in length was removed from each trunk to ensure complete denervation. The abdominal muscle layer and skin were then closed with sutures, and the wound was disinfected. Mice were allowed a 5-day recovery period before any subsequent experimental procedures.

Labeling of Fos^{dBNST} neurons

For specific labeling of Fos^+ neurons in the dBNST, Fos-$CreER^{T2}$ x Rosa-TdT transgenic mice were used. Immediately after intraperitoneal LPS injection, mice received intraperitoneal 4-OHT (Sigma, cat. no. H6278) at 25 mg/kg to label neurons activated during the inflammatory response with TdTomato. 4-OHT was freshly prepared before administration by dissolving it in corn oil and ethanol at a 9:1 volume ratio.

Retrograde tracing

For retrograde tracing, mice were anesthetized with 1.25% tribromoethanol (0.2 mL/10 g body weight) and placed supine on a temperature-controlled warming platform maintained at approximately 37°C. The limbs were extended and secured with conductive tape to expose the abdomen. Abdominal fur was removed, the surgical area was disinfected with iodophor, and a midline abdominal incision was made with sterile surgical scissors to expose the spleen.

Two retrograde tracers were used: the polysynaptic tracer PRV-CAG-EGFP (Braincase, Shenzhen) and the monosynaptic tracer red retrobeads (Lumafluor). A microsyringe fitted with a trimmed glass micropipette was loaded with the tracer: PRV-CAG-EGFP was injected at 200 nL per site across four sites, and red retrobeads were injected at 2 μL per site across four sites. Under stereomicroscopic visualization, the spleen was gently retracted and stabilized with cotton-wrapped forceps moistened with sterile saline to prevent desiccation and mechanical damage. The microsyringe was inserted into the splenic submucosa, and tracer was delivered at 100 nL/min. After

injection, the microsyringe was held in place for 5 min to allow diffusion and minimize reflux, then slowly withdrawn. The abdominal wound was sutured and disinfected with iodophor. Seven days later, mice were euthanized, and 30-μm brain sections were prepared for confocal imaging of fluorescently labeled neuronal populations.

Fiber Photometry

Neuronal Calcium Imaging

AAV-hSyn-GCaMP6s was injected into the dBNST, and an optical fiber was implanted ipsilaterally. Recordings were performed after a 2-week recovery period. Fluorescence signals were acquired using a fiber photometry system (THINKERTECH, China) at 50 Hz. The output power of the 470-nm LED was adjusted to maintain radiant flux at the fiber tip between 20 and 40 μW. Mice were acclimated to the recording environment for 1 h before recording and were allowed to move freely during acquisition. Calcium signals were expressed as dF/F0 = (F - F0)/F0, where F0 was the mode value of the entire recording session. Accumulated calcium events were defined as events with peak amplitudes exceeding twice the mean cumulative fluorescence intensity. A within-subject design was used. Mice first received intraperitoneal sterile saline followed by a 20-min baseline recording; 24 h later, the same mice received intraperitoneal LPS (50 μg/kg), followed by a second 20-min recording. For astrocyte activation combined with neuronal calcium imaging, mice were co-injected with AAV-GfaABC1D-DIO-hM3Dq-mCherry and AAV-hSyn-GCaMP6s, with simultaneous optical fiber implantation. After 3 weeks of recovery, mice received intraperitoneal LPS

(50 μg/kg) and 4-OHT to label Fos^{dBNST} astrocytes and induce hM3Dq expression. After an additional 2-week recovery period, neuronal calcium activity was recorded after intraperitoneal saline as a control; 24 h later, CNO (3 mg/kg) was administered intraperitoneally, and neuronal calcium signals were recorded to assess the effect of astrocyte activation on neuronal excitability.

Astrocytic ATP and Glutamate Detection

Mice received dBNST injections of either the astrocyte-specific ATP probe rAAV-GfaABC1D-ATP1.0-L or the glutamate probe rAAV-GfaABC1D-iGluSnFR3.v857.GPI, followed by a 3-week recovery period. For experiments requiring local drug delivery in the glutamate-probe group, a guide cannula (AP +0.14 mm, ML +0.8 mm, DV -4.25 mm) and an optical fiber (AP +0.14 mm, ML +2.9 mm, DV -5 mm, 30° from vertical) were implanted ipsilaterally and secured with dental cement. Fluorescence acquisition and data analysis were performed as described above. Using a within-subject design, mice injected with either probe first received intraperitoneal saline followed by a 20-min baseline recording; 24 h later, LPS (50 μg/kg) was administered intraperitoneally, followed by a second 10-min recording to compare LPS-induced changes in ATP concentration and glutamate release. For local drug delivery, an injection cannula connected via PE-10 tubing to a 5-μL Hamilton syringe was inserted through the guide cannula. Artificial cerebrospinal fluid (ACSF) (0.3 μL) was first injected as a vehicle control, followed by Adenosine 5'-O-(3-thiotriphosphate) (ATPγS) (50 μM, 0.3 μL) at the same site at 0.2 μL/min, with the

cannula left in place for 5 min to allow diffusion. In a separate cohort, MRS2179 (1 μg/0.3 μL) was locally injected before ATPγS (50 μM, 0.3 μL) to assess the effect of $P2Y_1$ receptor blockade. In another experiment, mice received intraperitoneal LPS (50 μg/kg) with local ACSF (0.3 μL) as a control; 24 h later, intraperitoneal LPS (50 μg/kg) was co-administered with local MRS2179 (1 μg/0.3 μL), and glutamate signals were recorded to evaluate $P2Y_1$ receptor involvement in LPS-induced glutamate release. All local injections were followed by a 5-min cannula-retention period.

Statistical analysis

Sample sizes were determined based on preliminary experiments and relevant literature. Mice were randomly assigned to experimental groups, with blinding implemented during operations and data collection. All data points represent independent biological replicates (individual animals), and no outliers were excluded.

All results are expressed as mean ± standard deviation. Normality was assessed using the Kolmogorov-Smirnov test. Parametric data were analyzed using an unpaired two-tailed t-test for two-group comparisons and one-way or two-way ANOVA for experiments with three or more groups or factorial designs. Non-parametric data were analyzed using the Wilcoxon test for two-group comparisons or the Kruskal-Wallis test for multiple-group comparisons. $P < 0.05$ was considered statistically significant. All analyses were performed using GraphPad Prism 9.5.1.

4.Results

4.1 Activation of Fos^{dBNST} Neurons by LPS-induced immune Responses and the Underlying Mechanisms.

Although multiple brain regions have been implicated in immune regulation, the specific neuronal populations involved remain incompletely defined. To address this question, we used LPS to induce an innate immune response in mice and examined the neuronal populations and functional changes associated with immune modulation. Animals were randomly assigned to receive intraperitoneal LPS or sterile saline (Fig. 1A). Because previous studies indicate that serum inflammatory cytokines peak approximately 3 hours after intraperitoneal LPS injection in mice[5], peripheral blood was collected at this time point. A single intraperitoneal injection of LPS significantly increased serum IL-1β and TNF-α levels (Fig. 1B, C), confirming successful induction of peripheral immune responses. To further characterize the immune response, we analyzed the changes in innate immune subsets in the peripheral blood and spleen following LPS stimulation. Flow cytometry revealed marked changes in leukocyte dynamics (Fig. S1A, B), including altered proportions of neutrophils, Ly-$6C^{high}$ monocytes, and macrophages in LPS-treated mice compared with saline-treated controls, the frequencies of T and B lymphocytes in peripheral blood and spleen did not differ significantly between groups (Fig. 1D, E). We also recorded splenic nerve activity using tungsten electrodes placed on splenic nerve fibers (Fig. S2A). LPS significantly increased splenic nerve firing frequency (Fig. S2B, C), indicating that systemic immune activation is accompanied by activation of splenic neural innervation.

Together, these results confirm that intraperitoneal LPS induces peripheral immune response and concurrently enhances splenic nerve activity.

We next used Fos, an immediate early gene, as a marker of neuronal activation to map brain regions recruited during LPS-induced immune dysregulation (Fig. 1F). LPS activated multiple brain regions, including the dBNST, PVN, CeA, parabrachial nucleus (PB), locus coeruleus (LC), arcuate hypothalamic nucleus (Arc), and dorsomedial hypothalamic nucleus (DMH) (Fig. 1G, H). These results indicate that LPS stimulation activated multiple brain regions containing neuronal populations that participate in the regulation of inflammatory responses. Among the activated regions identified in the c-Fos screen, the dBNST drew our particular attention. This nucleus is situated at the forebrain-midbrain junction and projects to brainstem autonomic nuclei[36], possessing the anatomical conditions for conveying forebrain information to the brain-spleen axis. Previous studies have implicated this region in inflammation regulation, but the underlying mechanisms remain unclear. We therefore focused our subsequent investigations on the dBNST to elucidate the cellular and circuit mechanisms through which it modulates periphercal immunity.

To determine how inflammatory stimuli activate Fos^{+} neurons in the dBNST, we examined both neural and humoral routes. We first examined whether the vagus nerve mediates the activation of dBNST neurons by monitoring real-time calcium dynamics with fiber photometry (Fig. 2A). Compared with saline, LPS significantly increased GCaMP6s fluorescence in dBNST neurons (Fig. 2B-H). However, when the same mice

were subjected to vagotomy and then re-injected with LPS, the area under the curve (AUC), DeltaF/F, and frequency recorded by fiber photometry were all significantly reduced compared with the LPS group, with the reduction exceeding half (Fig. 2B–H). Immunofluorescence further showed that vagotomy significantly reduced the number of Fos-positive neurons in the dBNST compared with sham-operated controls (Fig. S3A, B). These results suggest that LPS increases dBNST neuronal activity and that this effect is partially dependent on vagal signaling. We next examined whether humoral inflammatory signals also contribute to dBNST activation. Previous experiments confirmed that intraperitoneal injection of LPS significantly elevated serum IL-1β and TNF-α levels (Fig. 1B, C), and these cytokines have been reported to activate neurons in specific brain regions[4]. To test whether IL-1β and TNF-α activate dBNST neurons that are connected to the spleen, we combined $CreER^{T2}$ x Rosa-TdT mice (Fig. S4) with splenic injection of PRV-EGFP for retrograde tracing (Fig. 2I). Mice received intraperitoneal saline, LPS, or IL-1β+TNF-α, together with 4-OHT to label activated Fos^{dBNST} neurons. Compared with saline, IL-1β+TNF-α significantly increased the number of spleen-projecting Fos^{dBNST} neurons; however, LPS induced a larger spleen-projecting Fos^{dBNST} population than cytokines alone (Fig. 2J, K).

Together, these results indicate that peripheral LPS stimulation activates the dBNST through both vagus nerve-mediated neural transmission and IL-1β/TNF-α-mediated humoral signaling, thereby enhancing dBNST neuronal excitability and contributing to the regulation of innate immune responses.

4.2 Inhibition of Fos^{dBNST} neurons attenuates LPS-induced Peripheral Immune Response.

To validate the role of Fos^{dBNST} neurons in LPS-induced immune dysregulation, we used chemogenetic and optogenetic approaches to inhibit LPS-activated Fos^{+} neurons in the dBNST and then assessed peripheral immune parameters. Using DOX-dependent labeling, we tagged LPS-activated Fos^{dBNST} neurons and administered CNO 1 hour before LPS challenge to silence these neurons (Fig. 3A). Chemogenetic silencing significantly reduced serum IL-1β and TNF-α levels (Fig. 3B, C), decreased the numbers of neutrophils, Ly-$6C^{high}$ monocytes, and macrophages in the spleen and peripheral blood (Fig. 3D, E), and left T and B lymphocyte numbers unchanged (Fig. S5A, B). Splenic nerve firing frequency was also significantly reduced (Fig. 3E). We next performed an independent optogenetic inhibition experiment. Fos-Cre-dependent virus was injected into the dBNST with optical fiber implantation; after LPS and 4-OHT administration to label Fos^{dBNST} neurons, mice were rechallenged with LPS and received light illumination to inhibit these neurons (Fig. 3F). Optogenetic inhibition similarly reduced serum IL-1β and TNF-α levels (Fig. 3G, H), decreased neutrophils, Ly-$6C^{high}$ monocytes, and macrophages in spleen and peripheral blood (Fig. 3I, J), did not alter T or B lymphocyte counts (Fig. S5C, D), and reduced splenic nerve firing rate (Fig. 3J).

These findings indicate that Fos^{dBNST} neuron activation contributes to LPS-induced immune dysregulation, and that suppressing these neurons attenuates innate

immune-cell imbalance, pro-inflammatory cytokine release, and splenic nerve hyperactivity.

4.3 Reactivation of Fos^{dBNST} Neuronal Ensembles Captured During LPS-Induced Immune Responses Recapitulates Immune Dysregulation

Given that the above inhibition experiments suggested the involvement of Fos^{dBNST} neurons in LPS-induced immune dysregulation, we next asked whether reactivation of these neurons is sufficient to alter immune phenotypes. We used the DOX-controlled tTA system to label LPS-activated Fos^{dBNST} neurons and reactivated them with CNO after a recovery period (Fig. 4A). Chemogenetic reactivation alone did not produce obvious changes in serum IL-1β or TNF-α levels. However, when reactivation was followed by LPS challenge, mice in the activation group showed significantly higher serum IL-1β and TNF-α levels than controls (Fig. 4B, C). Notably, in the absence of LPS stimulation, chemogenetic reactivation of these Fos^{dBNST} neurons alone was sufficient to increase the numbers of neutrophils, Ly-6C^{high} monocytes, and macrophages in peripheral blood and spleen (Fig. 4D, E), whereas T and B lymphocyte numbers remained unchanged (Fig. S5E, F). Splenic nerve firing frequency was significantly elevated as well (Fig. 4E).

We further confirmed these findings using an independent optogenetic strategy. LPS-activated Fos^{dBNST} neurons were labeled using the Fos-Cre system and 4-OHT administration and were subsequently activated by 470-nm light stimulation (Fig. 4F). After optogenetic activation, subsequent LPS challenge significantly increased serum

IL-1β and TNF-α levels (Fig. 4G, H). In parallel, in the absence of LPS stimulation, optogenetic activation of these Fos^{dBNST} neurons alone similarly caused a significant increase in the number of neutrophils, Ly-$6C^{high}$ monocytes, and macrophages in peripheral blood and spleen (Fig. 4I, J), whereas T and B lymphocyte counts were unchanged (Fig. S5G, H). Splenic nerve firing frequency was also elevated (Fig. 4J).

Together, these results demonstrate that reactivation of Fos^{dBNST} neuronal ensembles captured during LPS-induced immune responses, even in the absence of LPS stimulation, is sufficient to induce increases in innate immune-cell in the peripheral blood and spleen. This pattern is consistent with the immune cell subset changes observed following LPS injection. Upon subsequent LPS exposure, these reactivated neuronal ensembles further amplify pro-inflammatory cytokine release.

4.4 Fos^{dBNST} Neurons Regulate Immune Responses via the dBNST-DVC-Spleen Neural Circuit

To determine whether Fos^{dBNST} neurons regulate immune responses through defined neural circuits, we first injected EGFP-expressing PRV into the mouse spleen to label brain regions directly or indirectly connected to the spleen through polysynaptic retrograde tracing (Fig. 5A). PRV-labeled regions included the PVN, dBNST, DVC, parasubthalamic nucleus (PSTh), parvicellular reticular formation-alpha(PCRtA), CeA, periaqueductal gray (PAG), and LC (Fig. 5B, C). To identify direct projection sources to the spleen, we injected red retrobeads into the spleen for monosynaptic retrograde tracing (Fig. 5D). Retrobead-labeled neurons were predominantly concentrated in the

DVC, and Choline acetyltransferase (ChAT) immunofluorescence showed that approximately 80% of spleen-projecting DVC neurons were cholinergic (Fig. 5E, F). To test whether LPS-activated Fos^{dBNST} neurons project to the DVC, red retrobeads were injected into the DVC; one week later, mice received intraperitoneal LPS or sterile saline (Fig. 5G). Immunofluorescence showed that LPS significantly increased the number of DVC-projecting Fos^{dBNST} neurons compared with controls (Fig. 5H), confirming that immune stimulation recruits dBNST neurons within the dBNST-DVC pathway.

We next tested the functional connectivity of this pathway. To test whether Fos^{dBNST} neurons can directly drive splenic output, we optogenetically activated them while recording splenic nerve activity. (Fig. 5I). Real-time splenic nerve recordings showed no baseline difference between groups before stimulation. During 470-nm light stimulation, splenic nerve firing increased in the ChR2 group but not in GFP controls, and firing returned to baseline after light offset (Fig. 5J, K). To assess the specific contribution of the dBNST-DVC projection, the same viral strategy was used in the dBNST while an optical fiber was implanted in the DVC to stimulate axon terminals of dBNST neurons projecting to the DVC (Fig. 5L). Terminal stimulation significantly increased splenic nerve firing in ChR2 mice compared with GFP controls, and firing again returned to baseline after stimulation ended (Fig. 5M, N), supporting functional connectivity of the Fos^{dBNST}-DVC-spleen pathway. We then tested whether this pathway regulates inflammatory responses. Optogenetic inhibition of Fos^{dBNST} axon

terminals in the DVC attenuated LPS-induced inflammation (Fig. 6A), as shown by reduced serum IL-1β and TNF-α levels (Fig. 6B, C), decreased neutrophils, Ly-6C^{high} monocytes, and macrophages in blood and spleen, and reduced splenic nerve firing (Fig. 6D, E). Conversely, optogenetic activation of Fos^{dBNST} terminals in the DVC altered immune-cell distribution (Fig. 6F); after LPS stimulation, the light-activated group showed increased serum IL-1β and TNF-α levels (Fig. 6G, H), increased neutrophils, Ly-6C^{high} monocytes, and macrophages in blood and spleen, and increased splenic nerve firing (Fig. 6I, J). Neither optogenetic inhibition nor activation affected T lymphocytes or B lymphocytes in the spleen or blood (Fig. S5I-L).

Together, these results demonstrate that Fos^{dBNST} neurons regulate systemic immune status through the Fos^{dBNST}-DVC-spleen neural circuit.

4.5 Fos^{dBNST} Astrocytes Are Involved in the Regulation of LPS-Induced Immune Responses

The above experiments identified immune-regulatory engram neurons in the dBNST. However, neuronal activity is strongly influenced by surrounding glial cells[37]. Astrocytes, the most abundant glial cell type in the central nervous system[38], can regulate neighboring neuronal excitability through gliotransmitter release[39]. We therefore asked whether dBNST astrocytes are recruited by immune stimulation and whether they modulate neuron activity under inflammatory conditions. To assess astrocytic responses to LPS, we performed immunofluorescence staining in the dBNST of LPS or saline treated mice using NeuN, Sox-9, and c-Fos. Sox-9 is a

570 lineage-specific transcription factor stably expressed in astrocytes and is suitable for
571 astrocyte quantification. The proportion of c-Fos^{+}/Sox-9^{+} double-positive cells among
572 Sox-9^{+} cells was significantly higher in LPS-treated mice than in saline-treated controls
573 (Fig. 7A, B), indicating that LPS activates a subpopulation of dBNST astrocytes. To
574 determine whether these astrocytes regulate dBNST neuronal activity, we combined c-
575 Fos-iCreER^{T2} mice with the astrocyte-specific chemogenetic virus AAV-GfaABC1D-
576 DIO-hM3Dq-mCherry to label LPS-activated Fos^{+} astrocytes after LPS and 4-OHT
577 administration and selectively reactivate them with CNO. Virus-labeled cells were
578 highly colocalized with GFAP, confirming astrocyte specificity (Fig. 7C). Reactivation
579 of immune-related astrocytes increased the number of c-Fos^{+} neurons in the dBNST
580 compared with controls. To further test astrocyte-to-neuron regulation, AAV-
581 GfaABC1D-DIO-hM3Dq-mCherry and the neuronal calcium indicator AAV-hSyn-
582 GCaMP6s were co-injected into the dBNST. After immune-activated Fos^{+} astrocytes
583 were labeled, fiber photometry was used to monitor dBNST neuronal calcium dynamics
584 during CNO-induced astrocyte reactivation (Fig. 7F, G). CNO significantly enhanced
585 dBNST neuronal calcium activity compared with the control (Fig. 7H-J).

586 We next evaluated whether reactivation of these astrocytes affects systemic
587 immune status. LPS-induced Fos^{dBNST} astrocytes were labeled and reactivated using the
588 same strategy (Fig. 7K), after which peripheral immune parameters were assessed.
589 Upon LPS stimulation, chemogenetic activation of Fos^{dBNST} astrocytes significantly
590 increased serum IL-1β and TNF-α levels (Fig. 6L, M) and increased neutrophils, Ly-

591 6C^{high} monocytes, and macrophages in the spleen and peripheral blood (Fig. 7N, O).
592 Splenic nerve firing frequency was also significantly elevated (Fig. 7O). Together,
593 these results demonstrate that LPS activates a subpopulation of dBNST astrocytes and
594 generates Fos^{dBNST} astrocytes; selective reactivation of these astrocytes enhances
595 dBNST neuronal activity and drives changes in peripheral immune-cell distribution,
596 inflammatory cytokine secretion, and splenic nerve activity. These findings suggest that
597 Fos^{dBNST} astrocytes participate in systemic immune regulation by modulating dBNST
598 neuronal function.

599 **4.6 The ATP-P2Y$_1$ Receptor Pathway Mediates Glutamate Release from**
600 **Astrocytes in the dBNST**

601 Because activation of Fos^{dBNST} astrocytes enhanced neuronal excitability, we next
602 investigated the molecular mechanism underlying astrocyte-mediated regulation of
603 neuronal activity. Previous biochemical studies showed that intraperitoneal LPS
604 increases ATP levels in the dentate gyrus and that elevated ATP can act through
605 astrocytic P2Y$_1$ receptors[34]. Whether ATP is increased locally in the dBNST, and
606 how this signal contributes to astrocyte-mediated neuronal regulation, remained unclear.
607 To address this, we injected the astrocyte-specific ATP probe rAAV-GfaABC1D-
608 ATP1.0-L into the dBNST and used fiber photometry to monitor ATP dynamics after
609 intraperitoneal LPS or saline injection (Fig. 8A). ATP levels near dBNST astrocytes
610 were significantly increased after LPS injection compared with saline (Fig. 8B–D),
611 indicating that LPS induces a local ATP increase in the dBNST. Because elevated ATP

612 can promote glutamate release through astrocytic $P2Y_1$ receptors[40], and glutamate is
613 a key transmitter through which astrocytes regulate neuronal excitability, we next
614 measured astrocytic glutamate signals using rAAV-GfaABC1D-iGluSnFR3.v857.GPI
615 (Fig. 8E). The injection of LPS similarly increased glutamate levels in dBNST
616 astrocytes (Fig. 8F-H).

617 To test whether elevated ATP causally promotes astrocytic glutamate release, we
618 injected the glutamate probe into the dBNST and implanted a cannula for local drug
619 delivery of ATPγS, a $P2Y_1$ receptor agonist, or MRS2179, a $P2Y_1$ receptor antagonist
620 (Fig. 8I). ATPγS significantly increased astrocytic glutamate levels, whereas MRS2179
621 suppressed the ATPγS-induced glutamate elevation (Fig. 8J-L). To determine whether
622 endogenous ATP mediates LPS-induced glutamate release through $P2Y_1$ receptors,
623 MRS2179 or ACSF was infused into the dBNST during intraperitoneal LPS
624 administration (Fig. 8M). MRS2179 significantly attenuated the LPS-induced elevation
625 of astrocytic glutamate levels (Fig. 8N-P). Immunofluorescence further showed that
626 MRS2179 treatment during LPS stimulation reduced the number of activated astrocytes
627 in the dBNST compared with ACSF-treated controls (Fig. 8Q, R).

628 Together, these results indicate that, under inflammatory conditions, dBNST
629 astrocytes promote glutamate release through the ATP-$P2Y_1$ receptor pathway, thereby
630 enhancing local neuronal excitability and mediating astrocytic regulation of dBNST
631 neuronal activity.

632 **5.Discussion**

This study identifies the dBNST as a forebrain hub that links peripheral inflammatory signals to systemic immune regulation. Our results support a model in which LPS-induced immune activation recruits Fos^{dBNST} neurons and Fos^{dBNST} astrocytes, peripheral immune information reaches the dBNST through both vagal and humoral routes, and dBNST output is transmitted to the spleen through a DVC-dependent autonomic pathway. At the local circuit level, selective reactivation of inflammation-associated Fos^{+} astrocytic ensembles is sufficient to enhance dBNST neuronal excitability. At the molecular level, we further found that inflammatory stimuli promote ATP release from dBNST astrocytes, which in turn facilitates glutamatergic signaling via $P2Y_1$ receptors, thereby increasing local neuronal output. These findings suggest that this general astrocytic signaling pathway operates in parallel with the inflammation-associated Fos^{+} astrocytic ensemble to coordinate dBNST function. Together, these findings extend the brain-spleen axis from predominantly brainstem-centered models to a forebrain neuron-astrocyte framework, in which immune information is encoded by coordinated cellular ensembles and translated into changes in splenic nerve activity, innate immune-cell distribution, and inflammatory cytokine release (Fig. 9).

A major implication of this work is that the dBNST may serve as a forebrain site for immune engram formation. Previous studies have shown that inflammation-associated neuronal ensembles in various brain regions can store and retrieve immune information [26, 27, 41]. Our findings add the dBNST to this emerging map of immune-

encoding brain regions; dBNST engram outputs through the DVC-spleen pathway. Activity-dependent labeling captured LPS-activated Fos^{+} neurons in the dBNST; silencing these neurons reduced pro-inflammatory cytokine levels, splenic nerve firing, and the accumulation of neutrophils, Ly-$6C^{high}$ monocytes, and macrophages in both blood and spleen, whereas reactivation od these ensembles shifted peripheral immune-cell distribution, increased splenic nerve activity, and enhanced cytokine responses after immune challenge (Fig.4B, C, G, H; Fig 6G, H). These data indicate that the LPS-responsive Fos^{dBNST} neuronal ensembles encode immune information. Recent work identified IL-1β-responsive sngram neurons in the BNST and detected changes in heart rate, core body temperatue, and serum IL-6 levels upon their reactivation[14]. While their study demonstrated cytokine-specific neural coding in the BNST, it did not examine direxT neural control of peripheral lymphoid organs. In contrast, our study extends this framework by establishing the dBNST as a forebrain node that directly engages the spleen through a defined dBNST-DVC-spleen circuit. Using polysynaptic and monosynaptic retrograde tracing from the spleen, we identified this anatomical pathway, and optogenetic manipulation confirmed its functional relevance: activation of Fos^{dBNST} neurons or their DVC-projecting terminals rapidly increased splenic nerve firing (Fig. 5I-N), whie inhibition attenuated LPS-induced innate immune cell redistribution and cytokine production. These findings provide direct evidence for a forebrain-to-spleen neural pathway, positioning the dBNST as a critical hub through which inflammatory and emotional states influence peripheral immunity. Because the

dBNST is interconnected with the amygdala[42], PVN[43], and PB[44], and contributes to sustained anxiety, fear-memory expression[17], persistent fear in post-traumatic stress disorder[45], and defensive responses to unpredictable threats[46], these inflammation-associated ensembles may provide a cellular substrate through which stress and emotional states exacerbate inflammatory relapse. Future studies should determine whether chronic stress persistently alters the excitability, ensemble composition, or retrieval threshold of Fos^{dBNST} neurons, and whether modulating these neurons can interrupt the cycle between stress and immune dysregulation.

The present study also clarifies how peripheral inflammatory information enters and exits this forebrain node. Peripheral immune signals are generally transmitted to the brain through neural and humoral pathways. Intraperitoneal LPS can activate vagal afferents that convey immune information to the brain[47], while circulating cytokines can act on the central nervous system directly or indirectly through the blood-brain barrier. For example, Interleukin-1 (IL-1) and IL-6 act on the arcuate nucleus to regulate body-fat metabolism[48], and Interleukin-10 (IL-10) enhances dopaminergic neuron activity in the ventral tegmental area and promotes dopamine release[49]. Our data indicate that both routes converge on the dBNST: vagotomy attenuated LPS-induced dBNST neuronal activation, whereas intraperitoneal IL-1β and TNF-α activated dBNST neurons that project toward the spleen. On the output side, the spleen is the largest secondary lymphoid organ and a major source of pro-inflammatory cytokines[50, 51], making it a plausible effector organ for dBNST-mediated immune

696 regulation. Stress is known to alter splenic morphology and immune-cell
697 composition[20], and chronic social stress can induce splenomegaly and increase
698 circulating monocytes[52]. Previous work in chronic pain models further showed that
699 stress-related regions such as the PVN and CeA can regulate T-cell distribution through
700 a PVN/CeA-DMV-spleen circuit[6]. Here, we identified a descending dBNST-DVC-
701 spleen circuit, and functional interrogation of this pathway confirmed its role in
702 regulating LPS-induced cytokine production, innate immune-cell distribution, and
703 spleenic nerve activity (Fig.5, 6) These findings define a descending dBNST-DVC-
704 spleen circuit through which the forebrain can regulate peripheral immune response,
705 providing a circuit-level explanation for how stress-related forebrain networks may
706 influence peripheral inflammatory status.

707 Beyond neuronal circuitry, our findings reveal an astrocytic mechanism that
708 amplifies immune information within the dBNST. Neuronal excitability is shaped by
709 surrounding glial cells[53], and astrocytes, the most abundant glial cell type in the
710 central nervous system[38], regulate neuronal activity through gliotransmitter release
711 and have recently been implicated in memory recall[32]. We found that LPS activated
712 a subset of dBNST astrocytes and that selective reactivation of these inflammation-
713 associated Fos^{+} astrocytes increased dBNST neuronal activity and altered peripheral
714 immune status. Thus, Fos^{dBNST} astrocytes may function as local modulators that convert
715 inflammatory cues into changes in neuronal ensemble excitability. At the molecular
716 level, inflammatory stimuli can increase brain ATP levels[33], and ATP released from

activated glial cells can act as an important upstream signal under inflammatory conditions[40]. $P2Y_1$, the most abundant P2Y receptor subtype in astrocytes[35], is a Gq-coupled metabotropic purinergic receptor expressed in brain regions including the olfactory bulb[54], cerebral cortex[55], and cerebellum[56]. Activation of $P2Y_1$ mobilizes intracellular calcium through the phospholipase (PLC) and inositol 1,4,5-trisphosphate (IP3) pathway and participates in gliotransmitter release[57], cell proliferation[58], and neurovascular coupling[59]. ATP can also promote glutamate release through astrocytic $P2Y_1$ receptors[60], thereby regulating the excitability of neighboring neurons[40]. Consistent with this pathway, astrocyte-specific ATP and glutamate probes combined with in vivo fiber photometry showed that LPS increased local ATP and astrocytic glutamate signals in the dBNST. The $P2Y_1$ receptor antagonist MRS2179 blocked LPS- or ATPγS-induced glutamate elevation, whereas the $P2Y_1$ receptor agonist ATPγS mimicked ATP-driven glutamate release. These results identify the ATP-$P2Y_1$ receptor-glutamate pathway as a molecular bridge between inflammatory cues, astrocyte activation, and neuronal excitability in the dBNST. This pathway may be physiologically useful for encoding immune information, but persistent activation could become maladaptive. In epilepsy models, $P2Y_1$-dependent glutamate release promotes neuronal hyperexcitability[61, 62], and patients with temporal lobe epilepsy show pro-inflammatory changes in peripheral T cells, B cells, monocytes, and NK cells, including elevated IL-6, TNF-α, Interferon-gamma (IFN-γ), and Interleukin-17A (IL-17A) with compensatory IL-10 production by regulatory T

cells[63]. In Alzheimer's disease, reactive astrocytes highly express $P2Y_1$ and show aberrant calcium signaling[64], accompanied by altered peripheral T-cell subsets and B-cell phenotypes[65]. These observations suggest that immune challenge-ATP release-$P2Y_1$ activation-gliotransmitter release-neuronal dysfunction may represent a shared neuroimmune motif. In the dBNST, this motif links astrocyte-neuron communication to peripheral immune regulation and may offer a translational entry point for targeting stress-related or chronic inflammatory immune dysregulation via astrocytic $P2Y_1$ signaling. Speculatively, this motif may extend beyond acute inflammation to neurological disorders in which astrocytic $P2Y_1$ signaling is aberrant, such as epolepsy and Alzheimer’s disease. In these conditions, local astrocytic dysfunction could, through the dBNST-DVC-spleen circuit, skew peripheral immunity, which in turn might feed back on central inflammatory milieus and perpetuate astrocytic abnormalities. Whether such a reciprocal circuit exists, and whether it contributes to disease progression, warrants future investigation.

Several limitations should be considered. First, the molecular and projection-defined heterogeneity of Fos^{dBNST} neurons remains unresolved, and future work should determine which neuronal subtypes are necessary or sufficient for immune encoding and output to the DVC-spleen pathway. Second, although the ATP-$P2Y_1$-glutamate axis explains how immune-activated astrocytes enhance neuronal excitability, downstream signaling events and synaptic mechanisms remain to be defined. Third, the present experiments establish that dBNST astrocytes can modulate acute immune

responses, but whether they contribute to long-term storage of immune information through synaptic plasticity, remodeling of the local synaptic microenvironment, or persistent changes in astrocyte state requires further investigation. Finally, future studies should test whether chronic stress, recurrent inflammation, or disease models alter the stability and retrieval of dBNST neuron-astrocyte immune ensembles.

In summary, this study defines a forebrain neuron-astrocyte mechanism for systemic immune regulation. It identifies the dBNST as a key node for immune information encoding, demonstrates that peripheral immune signals reach the dBNST through vagal and humoral routes, and shows that dBNST output regulates innate immunity through a dBNST-DVC-spleen circuit. It further reveals that immune stimulation recruits dBNST astrocytes and that ATP-$P2Y_1$ receptor-dependent glutamate release enables these astrocytes to enhance neuronal excitability. By linking immune engram-like neuronal ensembles, astrocyte signaling, and autonomic output to the spleen, these findings broaden the framework of forebrain-autonomic-immune organ communication and provide mechanistic insight into chronic inflammatory disease and stress-related immune dysregulation.

Acknowledgements

We thank the Translational Medicine Core Facility of Shandong University for consultation and instrument availability that supported this work.

Authors' contributions

Xijia Xin: Conceptualization, Methodology, Software, Data curation, Formal analysis, Writing-original draft. Yaqi Tang: Conceptualization, Methodology, Investigation. Mengdong Shi: Methodology, Validation. Weikai Han: Methodology, Investigation. Xi Xu: Validation. Chenyu Zhang: Validation. Tongtong Meng: Validation. Qingwei Yue: Investigation. E Liu: Conceptualization, Methodology, Supervision, Whiting-review & editing, Project administration, Funding acquisition. Jinhao Sun: Conceptualization, Methodology, Supervision, Whiting-review & editing, Project administration, Funding acquisition.

Funding

This work was supported by the National Nature Science Foundation (No.82471517, No.82401755), the Major Basic Research Project of Shandong Provincial Natural Science Foundation (No.ZR2025ZD05) and Shandong Provincial Natural Science Foundation (No.ZR2024QH204).

Data availability

All data supporting the conclusions of this study are included in the main text and/or the Supplementary information.

Declarations

Ethics approval and consent to participate

All animal experiments in this study were approved by the Institutional Animal Care and Use Committee at the Shandong University (No.IRB-SBMS-SDU(L)2026-02-2)

Consent for publication

All listed authors consent to the submission, and all data are used with the consnt of the person generating the data.

Competing interests

The authors declare no competing interests.

References

1. Bronte, V. and M.J. Pittet, The Spleen in Local and Systemic Regulation of Immunity. Immunity, 2023. 56(5): p. 1152.
2. Zhang, X., et al., Brain control of humoral immune responses amenable to behavioural modulation. Nature, 2020. 581(7807): p. 204-208.
3. Kressel, A.M., et al., Identification of a brainstem locus that inhibits tumor necrosis factor. Proc Natl Acad Sci U S A, 2020. 117(47): p. 29803-29810.
4. Jagot, F., et al., The parabrachial nucleus elicits a vigorous corticosterone feedback response to the pro-inflammatory cytokine IL-1β. Neuron, 2023. 111(15): p. 2367-2382.e6.
5. Jin, H., et al., A body-brain circuit that regulates body inflammatory responses. Nature, 2024. 630(8017): p. 695-703.
6. Zhu, X., et al., Somatosensory cortex and central amygdala regulate neuropathic pain-mediated peripheral immune response via vagal projections to the spleen. Nat Neurosci, 2024. 27(3): p. 471-483.
7. Poller, W.C., et al., Brain motor and fear circuits regulate leukocytes during acute stress. Nature, 2022. 607(7919): p. 578-584.
8. Lebow, M.A. and A. Chen, Overshadowed by the amygdala: the bed nucleus of the stria terminalis emerges as key to psychiatric disorders. Mol Psychiatry, 2016. 21(4): p. 450-63.
9. Bota, M., O. Sporns, and L.W. Swanson, Neuroinformatics analysis of molecular expression patterns and neuron populations in gray matter regions: the rat BST as a rich exemplar. Brain Res, 2012. 1450: p. 174-93.
10. Bienkowski, M.S. and L. Rinaman, Immune challenge activates neural inputs to the ventrolateral bed nucleus of the stria terminalis. Physiol Behav, 2011. 104(2): p. 257-65.
11. Yi, W., et al., A bed nucleus of stria terminalis neuronal ensemble mediates inflammation-induced sleep alterations in male mice. Brain Behav Immun, 2026. 136: p. 106574.
12. Wang, Y., et al., A bed nucleus of stria terminalis microcircuit regulating inflammation-associated modulation of feeding. Nat Commun, 2019. 10(1): p. 2769.

13. Zhang, J., et al., Projections from subfornical organ to bed nucleus of the stria terminalis modulate inflammation-induced anxiety-like behaviors in mice. Sci Adv, 2024. 10(48): p. eadp9413.
14. Hashimoto, O., et al., Central neurons encode interleukin-1β signals and mediate stress-induced inflammation. J Exp Med, 2026. 223(4).
15. Sánchez-Zavaleta, R., et al., GPR55 in the bed nucleus of stria terminalis modulates anxiety-like behavior, amphetamine self-administration and inflammatory response. Prog Neuropsychopharmacol Biol Psychiatry, 2025. 140: p. 111418.
16. Kim, S.Y., et al., Diverging neural pathways assemble a behavioural state from separable features in anxiety. Nature, 2013. 496(7444): p. 219-23.
17. Walker, D.L., L.A. Miles, and M. Davis, Selective participation of the bed nucleus of the stria terminalis and CRF in sustained anxiety-like versus phasic fear-like responses. Prog Neuropsychopharmacol Biol Psychiatry, 2009. 33(8): p. 1291-308.
18. Galluzzi, L., T. Yamazaki, and G. Kroemer, Linking cellular stress responses to systemic homeostasis. Nat Rev Mol Cell Biol, 2018. 19(11): p. 731-745.
19. Haykin, H. and A. Rolls, The neuroimmune response during stress: A physiological perspective. Immunity, 2021. 54(9): p. 1933-1947.
20. Dantzer, R., Neuroimmune Interactions: From the Brain to the Immune System and Vice Versa. Physiol Rev, 2018. 98(1): p. 477-504.
21. Gurfein, B.T., et al., Enriched environment and stress exposure influence splenic B lymphocyte composition. PLoS One, 2017. 12(7): p. e0180771.
22. Cano, G., et al., Characterization of the central nervous system innervation of the rat spleen using viral transneuronal tracing. J Comp Neurol, 2001. 439(1): p. 1-18.
23. Han, S., et al., The Bed Nucleus of the Stria Terminalis-Paraventricular Nucleus of the Hypothalamus Neural Circuit Regulates Neuropathic Pain Through the Brain-Spleen Axis. Neurosci Bull, 2025. 41(12): p. 2148-2166.
24. Liu, X., et al., Optogenetic stimulation of a hippocampal engram activates fear memory recall. Nature, 2012. 484(7394): p. 381-5.
25. Roy, D.S., et al., Brain-wide mapping reveals that engrams for a single memory are distributed across multiple brain regions. Nat Commun, 2022. 13(1): p. 1799.
26. Koren, T., et al., Insular cortex neurons encode and retrieve specific immune responses. Cell, 2021. 184(24): p. 5902-5915.e17.
27. Liu, E., et al., Hcn1-dependent engram neurons in the PVN encode gastric inflammatory sensitization. Sci Adv, 2026. 12(20): p. eaeb6961.
28. Khakh, B.S., On astrocyte-neuron interactions: Broad insights from the striatum. Neuron, 2025. 113(19): p. 3079-3107.
29. Endo, F., et al., Molecular basis of astrocyte diversity and morphology across the CNS in health and disease. Science, 2022. 378(6619): p. eadc9020.

30. Kol, A., et al., Astrocytes contribute to remote memory formation by modulating hippocampal-cortical communication during learning. Nat Neurosci, 2020. 23(10): p. 1229-1239.
31. Xin, Q., et al., Neuron-astrocyte coupling in lateral habenula mediates depressive-like behaviors. Cell, 2025. 188(12): p. 3291-3309.e24.
32. Williamson, M.R., et al., Learning-associated astrocyte ensembles regulate memory recall. Nature, 2025. 637(8045): p. 478-486.
33. Wu, Z., et al., A sensitive GRAB sensor for detecting extracellular ATP in vitro and in vivo. Neuron, 2022. 110(5): p. 770-782.e5.
34. Wang, H., et al., Stimulation of microglia leads to a rapid antidepressant effect by triggering astrocytic P2Y1Rs and promoting BDNF-mediated neurogenesis in the hippocampus. Brain Behav Immun, 2025. 128: p. 134-151.
35. Lohr, C., Role of P2Y receptors in astrocyte physiology and pathophysiology. Neuropharmacology, 2023. 223: p. 109311.
36. Dong, H.W. and L.W. Swanson, Organization of axonal projections from the anterolateral area of the bed nuclei of the stria terminalis. J Comp Neurol, 2004. 468(2): p. 277-98.
37. Won, W., et al., Astrocytes as Key Regulators of Neural Signaling in Health and Disease. Annu Rev Neurosci, 2025. 48(1): p. 251-276.
38. Akdemir, E.S., A.Y. Huang, and B. Deneen, Astrocytogenesis: where, when, and how. F1000Res, 2020. 9.
39. Lines, J., et al., The Duality of Astrocyte Neuromodulation: Astrocytes Sense Neuromodulators and Are Neuromodulators. J Neurochem, 2025. 169(4): p. e70054.
40. Ye, M., et al., NR2B-CaMKII signaling in the dentate gyrus driven by astrocytic P2Y1Rs mediates the antidepressant effect of low-dose LPS. Brain Behav Immun, 2026. 135: p. 106529.
41. Ren, Q., et al., Inhibition of Ephrin receptor signaling in the paraventricular nucleus attenuates psoriasis-like dermatitis via synaptic plasticity and immune homeostasis modulation. J Neuroinflammation, 2025. 22(1): p. 211.
42. Ren, J., et al., A Distinct Metabolically Defined Central Nucleus Circuit Bidirectionally Controls Anxiety-Related Behaviors. J Neurosci, 2022. 42(11): p. 2356-2370.
43. Johnson, S.B., et al., A Basal Forebrain Site Coordinates the Modulation of Endocrine and Behavioral Stress Responses via Divergent Neural Pathways. J Neurosci, 2016. 36(33): p. 8687-99.
44. Palmiter, R.D., The Parabrachial Nucleus: CGRP Neurons Function as a General Alarm. Trends Neurosci, 2018. 41(5): p. 280-293.
45. Grillon, C., et al., Increased anxiety during anticipation of unpredictable aversive stimuli in posttraumatic stress disorder but not in generalized anxiety disorder. Biol Psychiatry, 2009. 66(1): p. 47-53.

46. Goode, T.D., et al., Bed nucleus of the stria terminalis regulates fear to unpredictable threat signals. Elife, 2019. 8.
47. Rinaman, L., Visceral sensory inputs to the endocrine hypothalamus. Front Neuroendocrinol, 2007. 28(1): p. 50-60.
48. Schéle, E., et al., Inter-relation between interleukin (IL)-1, IL-6 and body fat regulating circuits of the hypothalamic arcuate nucleus. J Neuroendocrinol, 2013. 25(6): p. 580-9.
49. Ronström, J.W., et al., Interleukin-10 enhances activity of ventral tegmental area dopamine neurons resulting in increased dopamine release. Brain Behav Immun, 2023. 113: p. 145-155.
50. Lewis, S.M., A. Williams, and S.C. Eisenbarth, Structure and function of the immune system in the spleen. Sci Immunol, 2019. 4(33).
51. Huston, J.M., et al., Splenectomy inactivates the cholinergic antiinflammatory pathway during lethal endotoxemia and polymicrobial sepsis. J Exp Med, 2006. 203(7): p. 1623-8.
52. McKim, D.B., et al., Social Stress Mobilizes Hematopoietic Stem Cells to Establish Persistent Splenic Myelopoiesis. Cell Rep, 2018. 25(9): p. 2552-2562.e3.
53. Hamilton, N.B. and D. Attwell, Do astrocytes really exocytose neurotransmitters? Nat Rev Neurosci, 2010. 11(4): p. 227-38.
54. Doengi, M., J.W. Deitmer, and C. Lohr, New evidence for purinergic signaling in the olfactory bulb: A2A and P2Y1 receptors mediate intracellular calcium release in astrocytes. Faseb j, 2008. 22(7): p. 2368-78.
55. Fumagalli, M., et al., Nucleotide-mediated calcium signaling in rat cortical astrocytes: Role of P2X and P2Y receptors. Glia, 2003. 43(3): p. 218-03.
56. Amadio, S., et al., P2Y1 receptor switches to neurons from glia in juvenile versus neonatal rat cerebellar cortex. BMC Dev Biol, 2007. 7: p. 77.
57. Jacob, P.F., et al., P2Y1 receptor inhibits GABA transport through a calcium signalling-dependent mechanism in rat cortical astrocytes. Glia, 2014. 62(8): p. 1211-26.
58. Quintas, C., et al., P2Y receptors on astrocytes and microglia mediate opposite effects in astroglial proliferation. Purinergic Signal, 2011. 7(2): p. 251-63.
59. Xia, M. and Y. Zhu, Signaling pathways of ATP-induced PGE2 release in spinal cord astrocytes are EGFR transactivation-dependent. Glia, 2011. 59(4): p. 664-74.
60. Domercq, M., et al., P2Y1 receptor-evoked glutamate exocytosis from astrocytes: control by tumor necrosis factor-alpha and prostaglandins. J Biol Chem, 2006. 281(41): p. 30684-96.
61. Sukigara, S., et al., Expression of astrocyte-related receptors in cortical dysplasia with intractable epilepsy. J Neuropathol Exp Neurol, 2014. 73(8): p. 798-806.

62. Nikolic, L., et al., Role of astrocyte purinergic signaling in epilepsy. Glia, 2020. 68(9): p. 1677-1691.
63. Vieira É, L.M., et al., Peripheral leukocyte profile in people with temporal lobe epilepsy reflects the associated proinflammatory state. Brain Behav Immun, 2016. 53: p. 123-130.
64. Delekate, A., et al., Metabotropic P2Y1 receptor signalling mediates astrocytic hyperactivity in vivo in an Alzheimer's disease mouse model. Nat Commun, 2014. 5: p. 5422.
65. Singh, A.S., A.R. Naqvi, and M.T. Chanu, Microglial, astrocytic, oligodendrocyte, B-/T-cell and neutrophil dysregulation in neuroinflammation of Alzheimer's disease and related dementias. J Psychiatr Res, 2026. 195: p. 225-243.

Figure legends

Figure 1

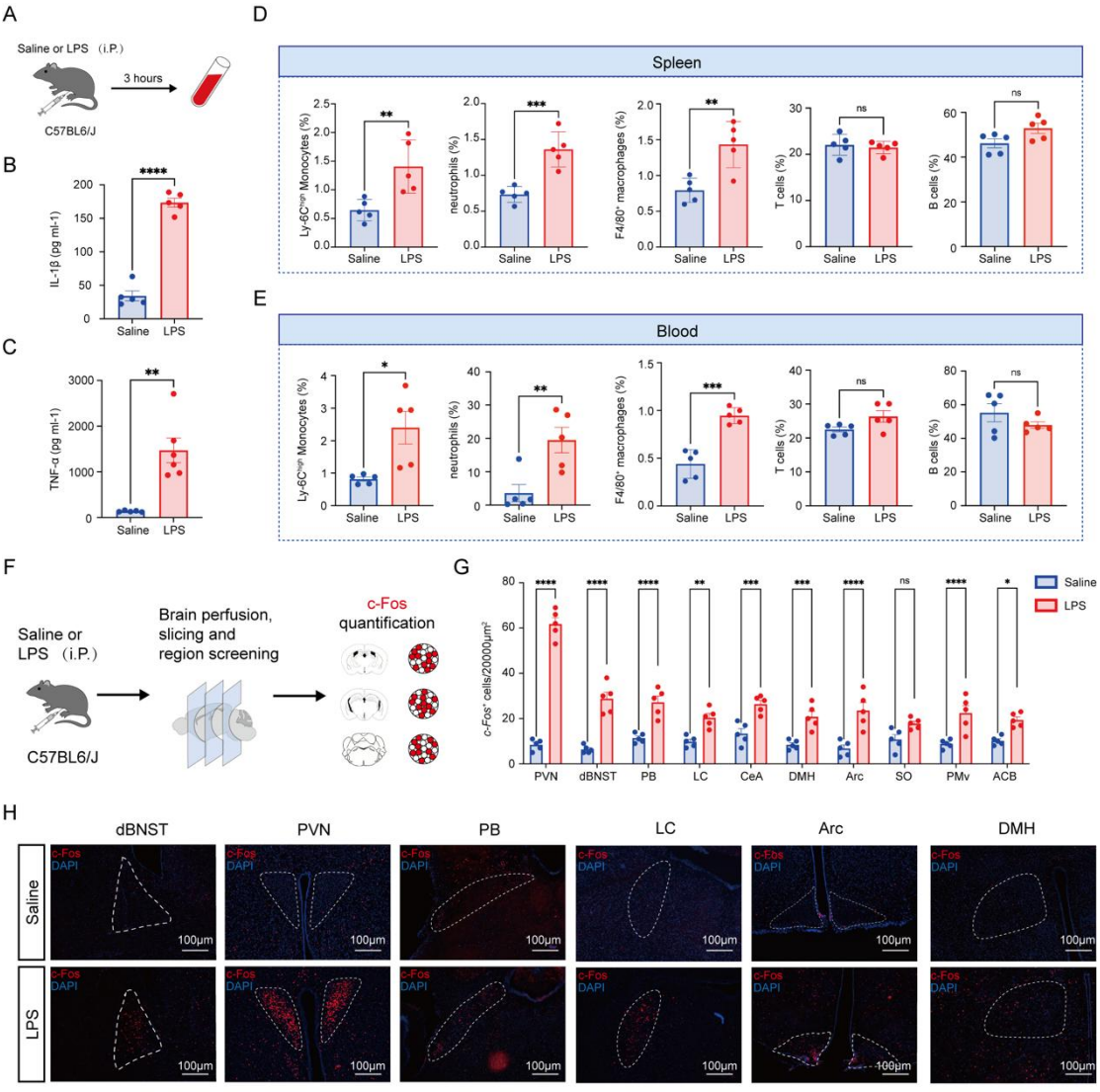
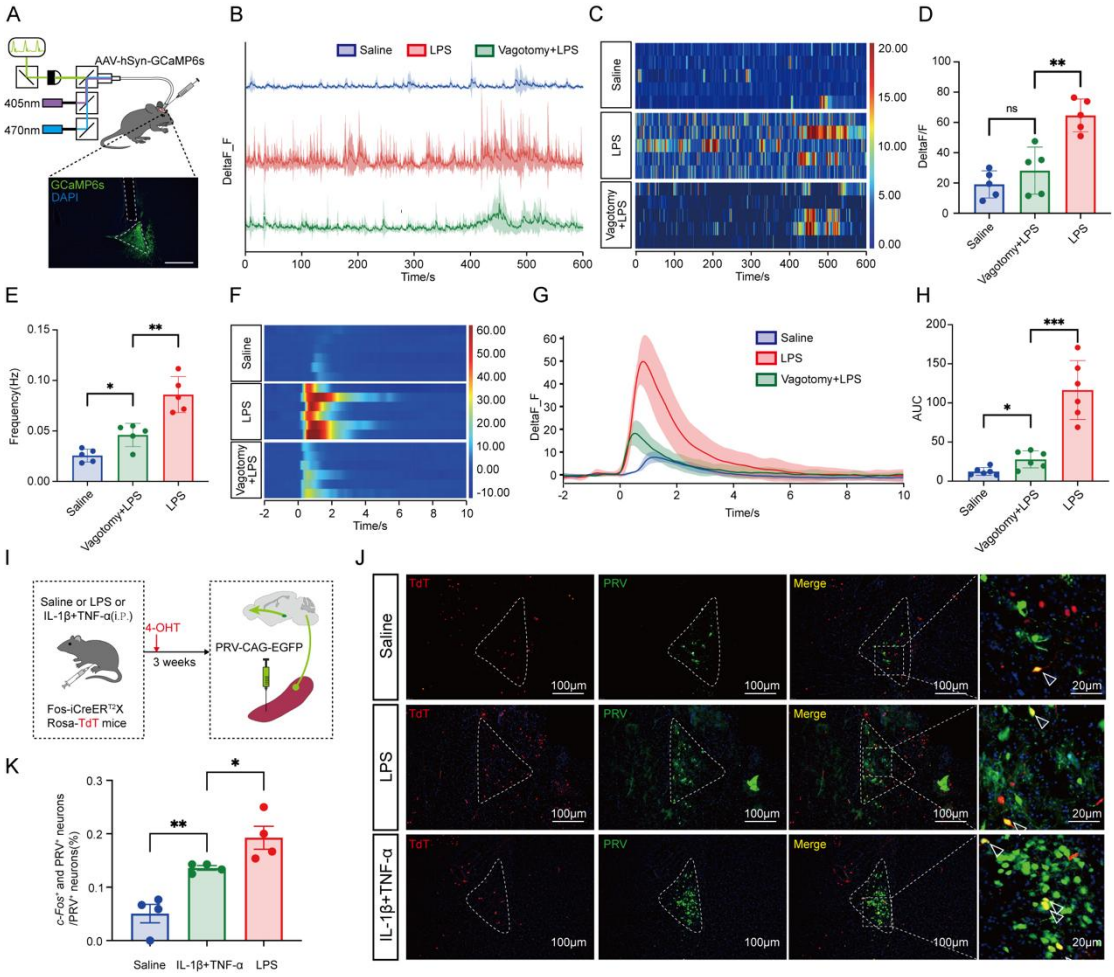


Figure 1. Intraperitoneal LPS injection induces peripheral immune responses and widespread neuronal c-Fos expression in the brain.

(A) Schematic depicting detection of LPS-triggered inflammatory cytokines and immune-cell populations. Wild-type mice received saline or LPS, and peripheral blood and spleen were sampled 3 h after injection. (B-C) Marked upregulation of IL-1β and TNF-α levels in peripheral blood (n=5; two-tailed t-test). (D-E) Altered immune-cell populations, including Ly-6C^{high} monocytes, neutrophils, macrophages, T cells, and B cells, in the spleen and peripheral blood (n=5; two-tailed t-test). (F) Schematic of Fos expression elicited by LPS challenge. Mice received intraperitoneal LPS or saline, and brains were immunostained for Fos expression 3 h later. (G) Mean number of Fos^{+} cells per brain region (n=5 per group; two-way ANOVA). *P<0.05, **P<0.01, ***P<0.001. (H) Representative Fos immunofluorescence images from saline- and LPS-treated mice.

Figure 2



988

989 **Figure 2. Activation Mechanism of Fos^{dBNST} Neurons in LPS-Induced Immune**

990 **Responses**

991 (A) Schematic diagram of the calcium imaging experimental setup. (B) In mice injected

992 with GCaMP6s AAV into the dBNST, neural responses were recorded following LPS

993 (red trace, n=5) and saline (blue trace, n=5) injections. Traces show mean (solid lines)

994 and s.e.m. (shaded areas). Green traces represent responses after bilateral vagotomy

995 (n=5). Saline and LPS injections were performed sequentially in the same animal. (C)

996 Heatmaps showing changes in neuronal activity in the LPS, saline, and vagotomy

997 groups during a 600-s recording period. (D-E) LPS induced increases in both amplitude

998 (ΔF/F) and frequency of calcium signals in dBNST neurons, whereas bilateral

vagotomy significantly attenuated this effect (n=5; one-way ANOVA). (F) Heatmaps showing neuronal activity patterns in each group of mice. (G) Average fluorescence intensity of dBNST neurons in each group. (H) LPS-induced increase in AUC of calcium signals in dBNST neurons (n=6, one-way ANOVA). (I) Fos-CreER^{T2} × Rosa-tdTomato mice were divided into three groups: saline group (intraperitoneal saline), IL-1β+TNF-α group (intraperitoneal IL-1β and TNF-α), and LPS group (intraperitoneal LPS). All three groups received concurrent intraperitoneal injections of 4-OHT during model establishment to label Fos-positive neurons activated during intraperitoneal injection. (J) Representative images showing co-localization of PRV with cytokine- or LPS-activated Fos^{+} dBNST neurons. (K) The co-localization rate of PRV with saline-activated Fos^{+} dBNST neurons was significantly lower than that with LPS-activated or cytokine-activated neurons (n=4; one-way ANOVA).

Figure 3

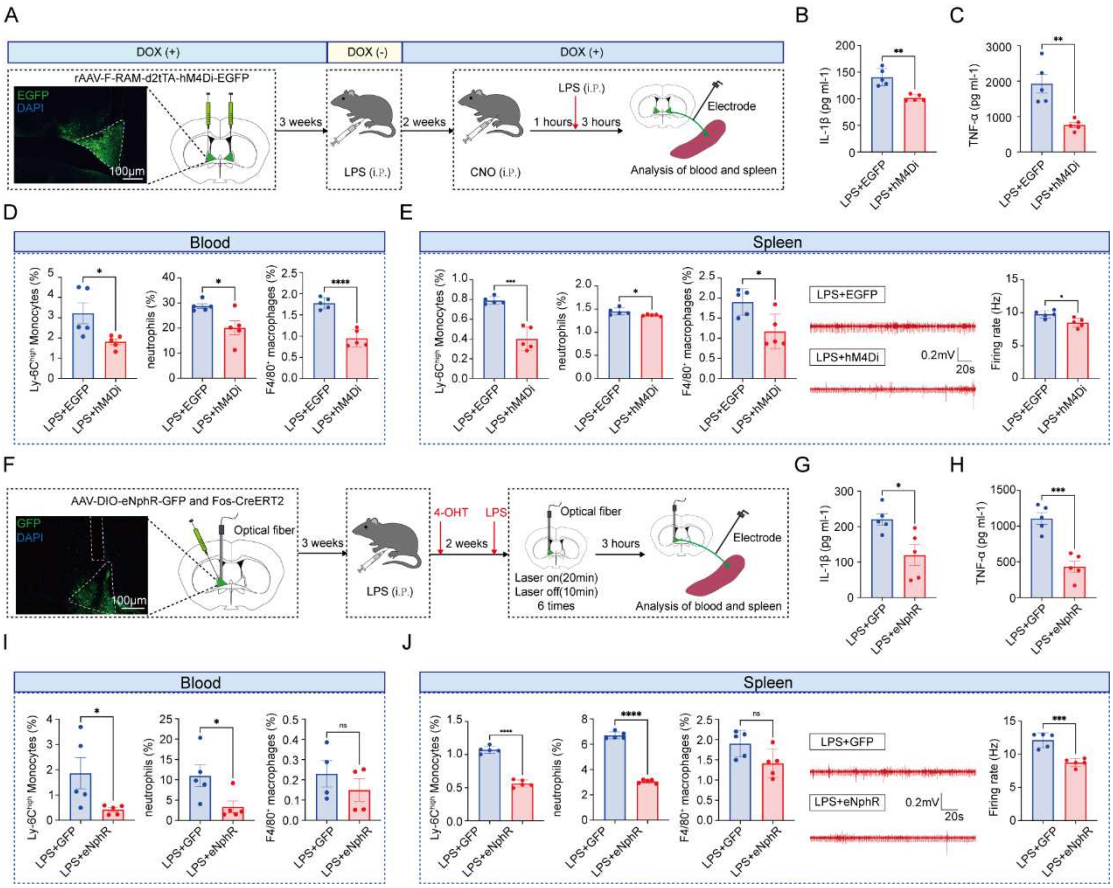


Figure 3. Inhibition of Fos^{dBNST} Neurons Attenuates LPS-Induced Immune Dysregulation

(A) Schematic of chemogenetic inhibition targeting LPS-activated Fos^{dBNST} neurons. rAAV-F-RAM-d2tTA-hM4Di-EGFP was injected into the dBNST. Mice were fed a DOX-supplemented diet for 3 weeks before modeling to enable labeling of LPS-activated Fos^{dBNST} neurons. After a 2-week recovery period, CNO (3 mg/kg) was injected intraperitoneally before LPS modeling to suppress Fos^{dBNST} neurons. (B-C) Chemogenetic inhibition of Fos^{dBNST} neurons attenuated LPS-associated inflammatory cytokine levels compared with controls (n=5; two-tailed t-test). (D-E) Chemogenetic inhibition reduced Ly-6C^{high} monocytes, neutrophils, and macrophages in the spleen and peripheral blood, and reduced splenic nerve firing frequency (n=5; two-tailed t-

test). (F) Schematic of optogenetic inhibition of Fos^{dBNST} neurons. (G-H) Optogenetic inhibition attenuated LPS-associated inflammatory cytokine levels compared with controls (n=5; two-tailed t-test). (I-J) Optogenetic inhibition reduced Ly-6C^{high} monocytes, neutrophils, and macrophages in the spleen and peripheral blood, and reduced splenic nerve firing frequency (n=5; two-tailed t-test).

Figure 4

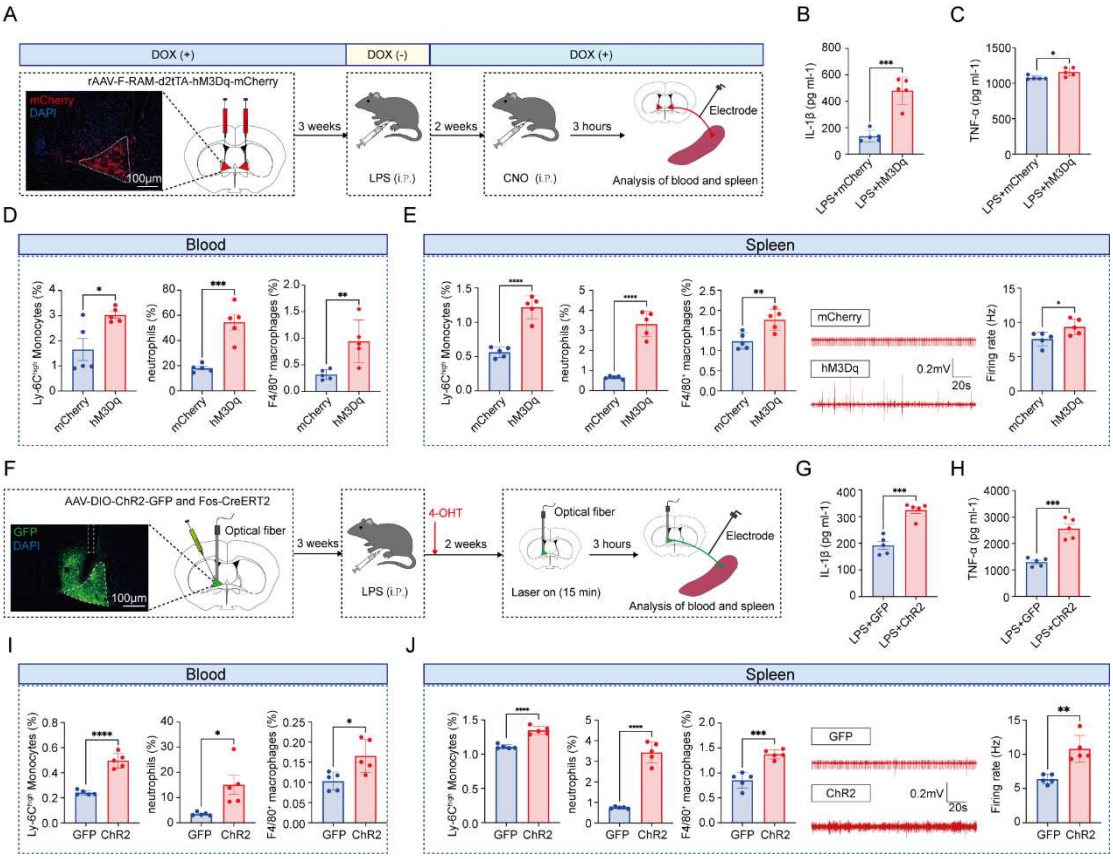


Figure 4. Reactivation of Fos^{dBNST} Neuronal Ensembles Captured During LPS-Induced Immune Responses Recapitulates Immune Dysregulation

(A) Schematic timeline for chemogenetic activation of Fos^{dBNST} neurons. rAAV-F-RAM-d2tTA-hM3Dq-mCherry was bilaterally injected into the dBNST. After 3 weeks of viral expression, mice received LPS to label LPS-activated Fos^{dBNST} neurons. After

a 2-week recovery period, CNO or saline was delivered intraperitoneally. (B-C) Chemogenetic activation of Fos^{dBNST} neurons increased LPS-associated inflammatory cytokine levels compared with controls (n=5; two-tailed t-test). (D-E) Chemogenetic activation increased Ly-$6C^{high}$ monocytes, neutrophils, and macrophages in the spleen and peripheral blood, and enhanced splenic nerve firing frequency (n=5; two-tailed t-test). (F) Schematic of optogenetic activation of Fos^{dBNST} neurons. (G-H) Optogenetic activation increased LPS-associated inflammatory cytokine levels compared with controls (n=5; two-tailed t-test). (I-J) Optogenetic activation increased Ly-$6C^{high}$ monocytes, neutrophils, and macrophages in the spleen and peripheral blood, and increased splenic nerve firing frequency (n=5; two-tailed t-test).

Figure 5

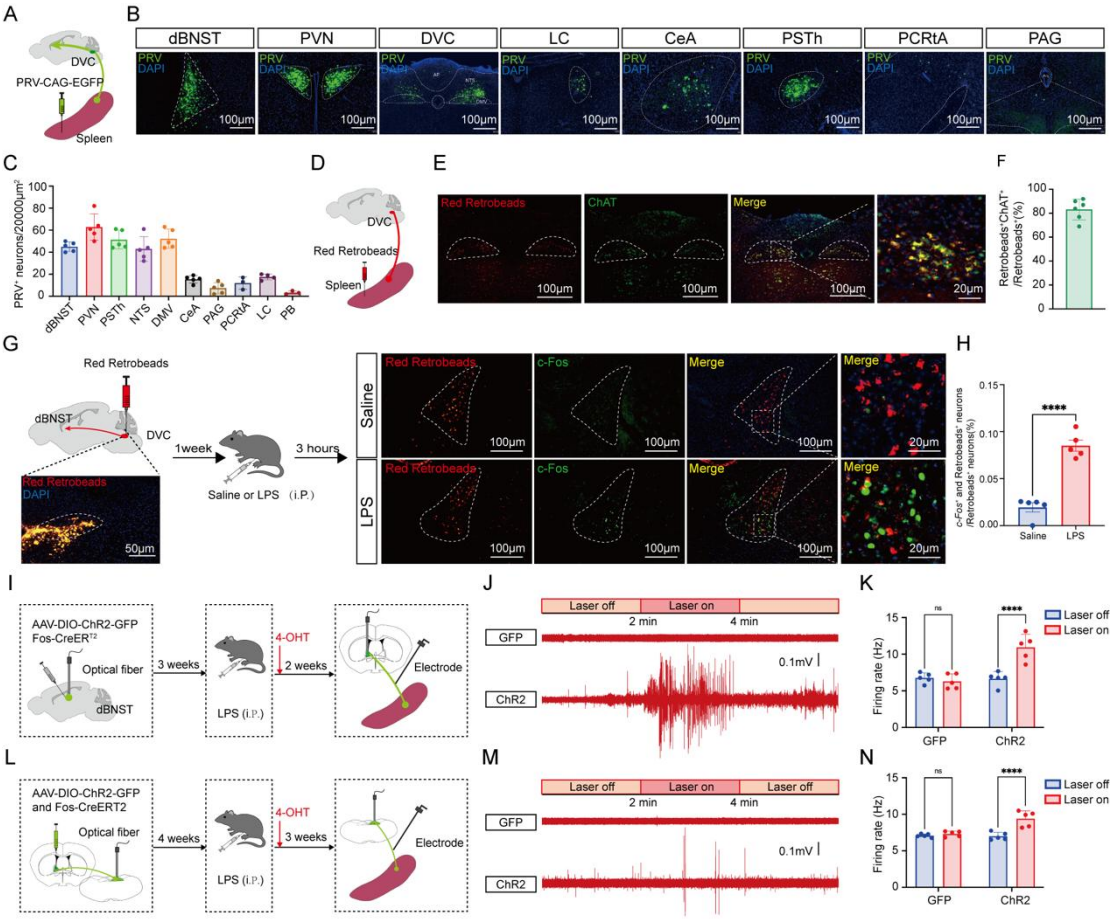


Figure 5. Fos^{dBNST} Regulates Immune Responses via the dBNST-DVC-spleen Neural Circuit

(A) Experimental scheme for spleen injection of PRV-CAG-EGFP. (B) Representative image showing whole-brain mapping of PRV-EGFP^{+} neurons. (C) Quantitative statistical results showing the number of PRV^{+} neurons in each brain region. (D) Experimental scheme for spleen injection of red retrobeads. (E) Representative image showing co-localization of retrobeads with ChAT^{+} neurons in the DVC. (F) Quantitative statistical results demonstrating that retrobead-labeled neurons predominantly overlapped with ChAT^{+} neurons (n=6). (G) Experimental scheme for DVC injection of red retrobeads. One week after injection, mice were divided into two

groups: the saline group received intraperitoneal saline, and the LPS group received intraperitoneal LPS. Three hours after injection, brains were immunostained for Fos. Representative images show retrobead-labeled neurons and Fos^+ neurons in the dBNST. (H) Statistical data showing the percentage of Fos^+ and $retrobead^+$ neurons among all retrobead-labeled neurons in the saline and LPS groups (n=5; two-tailed t-test). (I) Experimental design: optogenetic virus injection into the dBNST with fiber implantation for activation of the Fos^{dBNST}-spleen pathway and recording of splenic nerve firing frequency. (J-K) Optical stimulation of Fos^{dBNST} neurons significantly increased splenic nerve firing frequency (n=5; two-way ANOVA). (L) Experimental design: optogenetic virus injection into the dBNST and fiber implantation in the DVC for activation of axonal terminals of Fos^{dBNST} neurons projecting to the DVC, combined with recording of splenic nerve firing frequency. (M) Optical stimulation of axonal terminals of Fos^{dBNST} neurons in the DVC significantly increased splenic nerve firing frequency (n=5; two-way ANOVA).

Figure 6

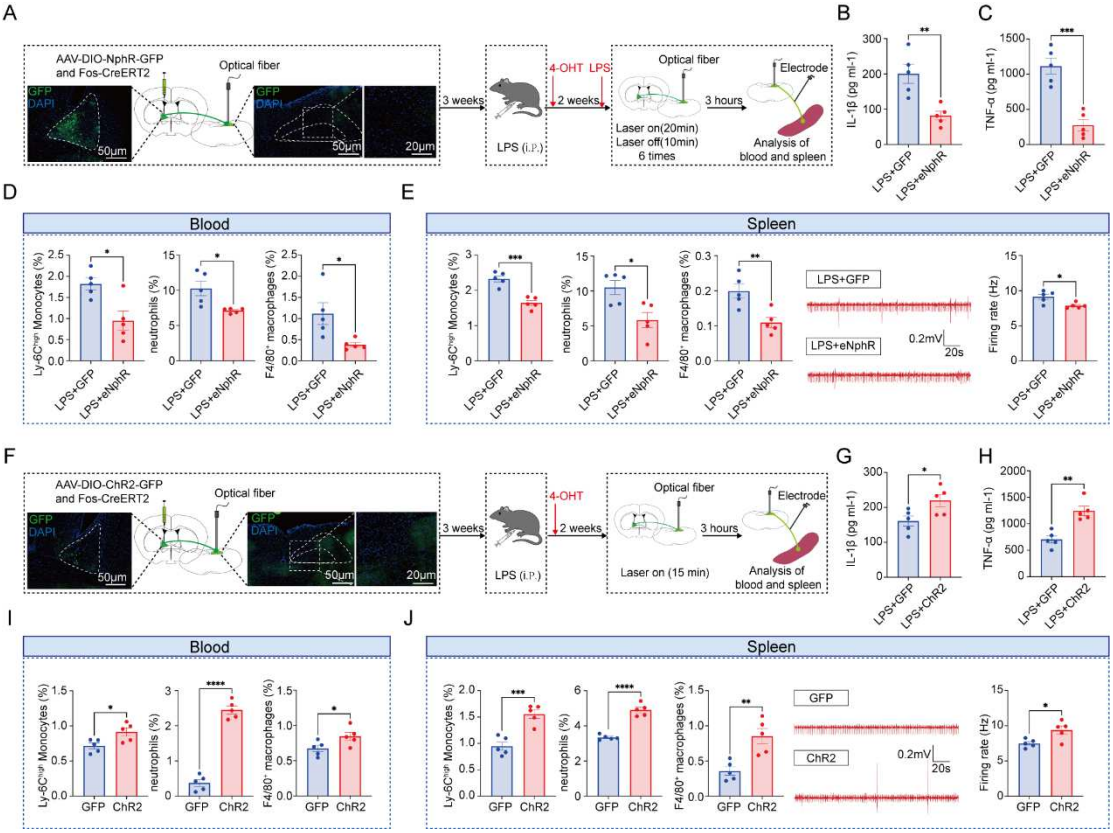


Figure 6. Optogenetic Manipulation of the Fos^{dBNST}-DVC Pathway Regulates Immune Responses

(A) Schematic of optogenetic inhibition of the Fos^{dBNST}-DVC pathway. (B-C) Optogenetic inhibition of the Fos^{dBNST}-DVC pathway attenuated LPS-associated inflammatory cytokine levels versus controls (n=5; two-tailed t-test). (D-E) Attenuated immune cells, including Ly-6C^{high} monocytes, neutrophils, and macrophages in the spleen and peripheral blood (n=5; two-tailed t-test). Reduced splenic nerve firing frequency following inhibition of the Fos^{dBNST}-DVC pathway (n=5; two-tailed t-test). (F) Schematic of optogenetic activation of the Fos^{dBNST}-DVC pathway. (G-H) Optogenetic activation of the Fos^{dBNST}-DVC pathway induced upregulation of LPS-associated inflammatory cytokine levels versus controls (n=5; two-tailed t-test). (I-J)

Elevated immune cells, including Ly-6C^{high} monocytes, neutrophils, and macrophages in the spleen and peripheral blood (n=5; two-tailed t-test). Increased splenic nerve firing frequency following activation of the Fos^{dBNST}-DVC pathway (n=5; two-tailed t-test).

Figure 7

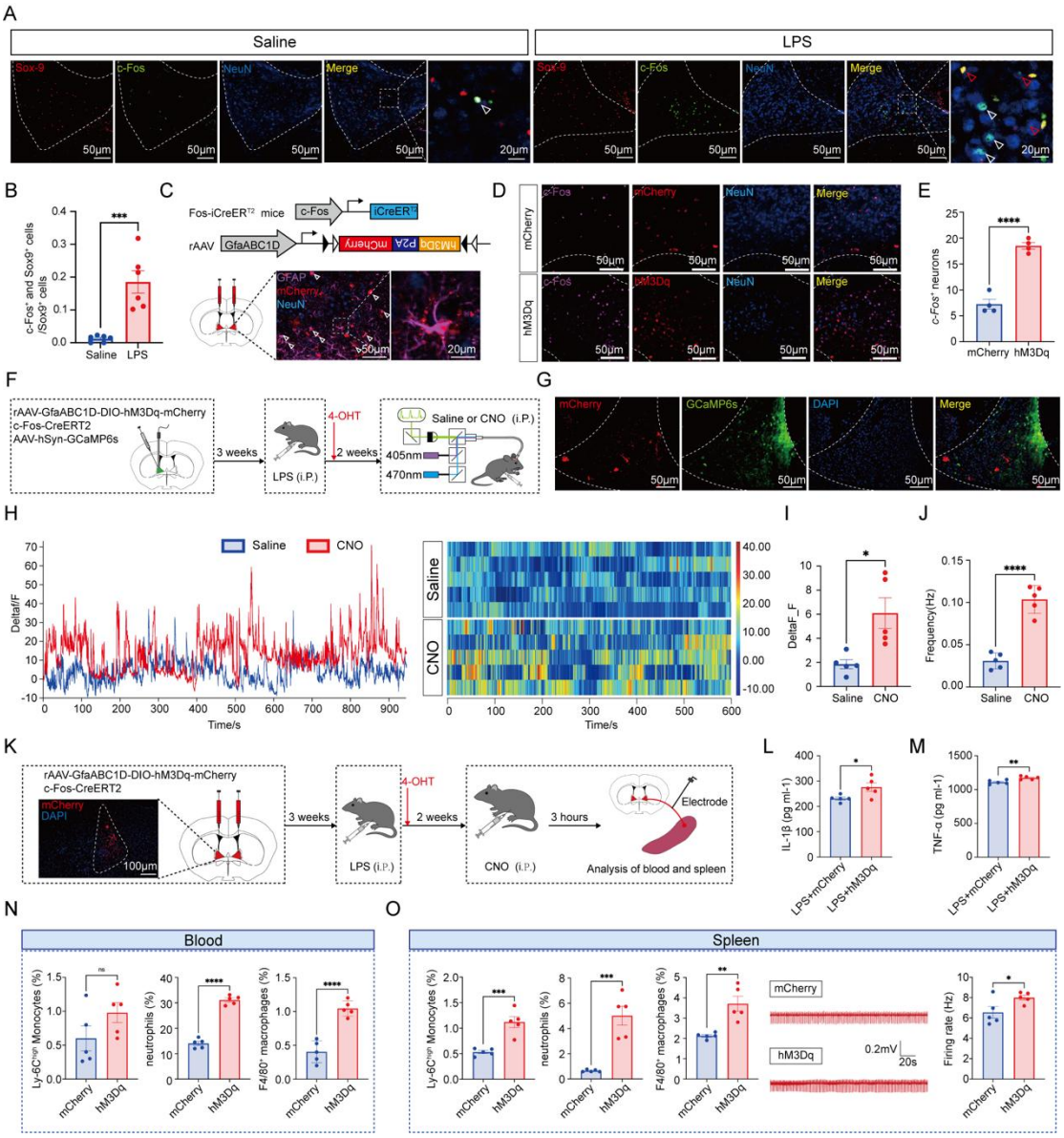


Figure 7. Fos^{dBNST} Astrocytes Are Involved in the Regulation of LPS-Induced Immune Responses

(A) Mice were given intraperitoneal administration of LPS or saline. Three hours later, brains were harvested for immunofluorescent staining of Sox-9, Fos, and NeuN. Representative images of the saline and LPS groups are shown. (B) LPS-induced immune activation significantly increased the number of activated astrocytes in the dBNST compared with the saline-treated group (n=6; two-tailed t-test). (C) Schematic of AAV construction and representative images. (D) Representative images showing c-Fos expression in the dBNST upon chemogenetic activation of Fos^{dBNST} astrocytes. (E) Chemogenetic activation of Fos^{dBNST} astrocytes increased the number of activated neurons in the dBNST (n=4; two-tailed t-test). (F-G) Experimental scheme for chemogenetic activation of Fos^{dBNST} astrocytes and detection of neuronal calcium activity, along with representative images showing virus injection sites. (H-J) Representative raw traces (H, left), heatmaps (H, right), and bar graphs (I, J) showing changes in calcium activity of dBNST neurons following chemogenetic activation of Fos^{dBNST} astrocytes (n=5; two-tailed t-test). (K) Experimental timeline for chemogenetic activation of Fos^{dBNST} astrocytes: the chemogenetic effector virus rAAV-GfaABC1D-DIO-hM3Dq-mCherry together with c-Fos-$CreER^{T2}$ was bilaterally injected into the dBNST. Following a 3-week period for viral expression, both groups of mice were injected with LPS and 4-OHT to label LPS-activated Fos^{dBNST} astrocytes. After a 2-week recovery period, CNO or saline was administered intraperitoneally. (L-M) Chemogenetic activation of Fos^{dBNST} astrocytes upregulated LPS-associated inflammatory cytokine levels versus controls (n=5; two-tailed t-test). (N, O) Elevated

immune cells, including Ly-6C^{high} monocytes, neutrophils, and macrophages in the spleen and peripheral blood (n=5; two-tailed t-test). Enhanced splenic nerve firing frequency following Fos^{dBNST} astrocytes activation (n=5; two-tailed t-test).

Figure 8

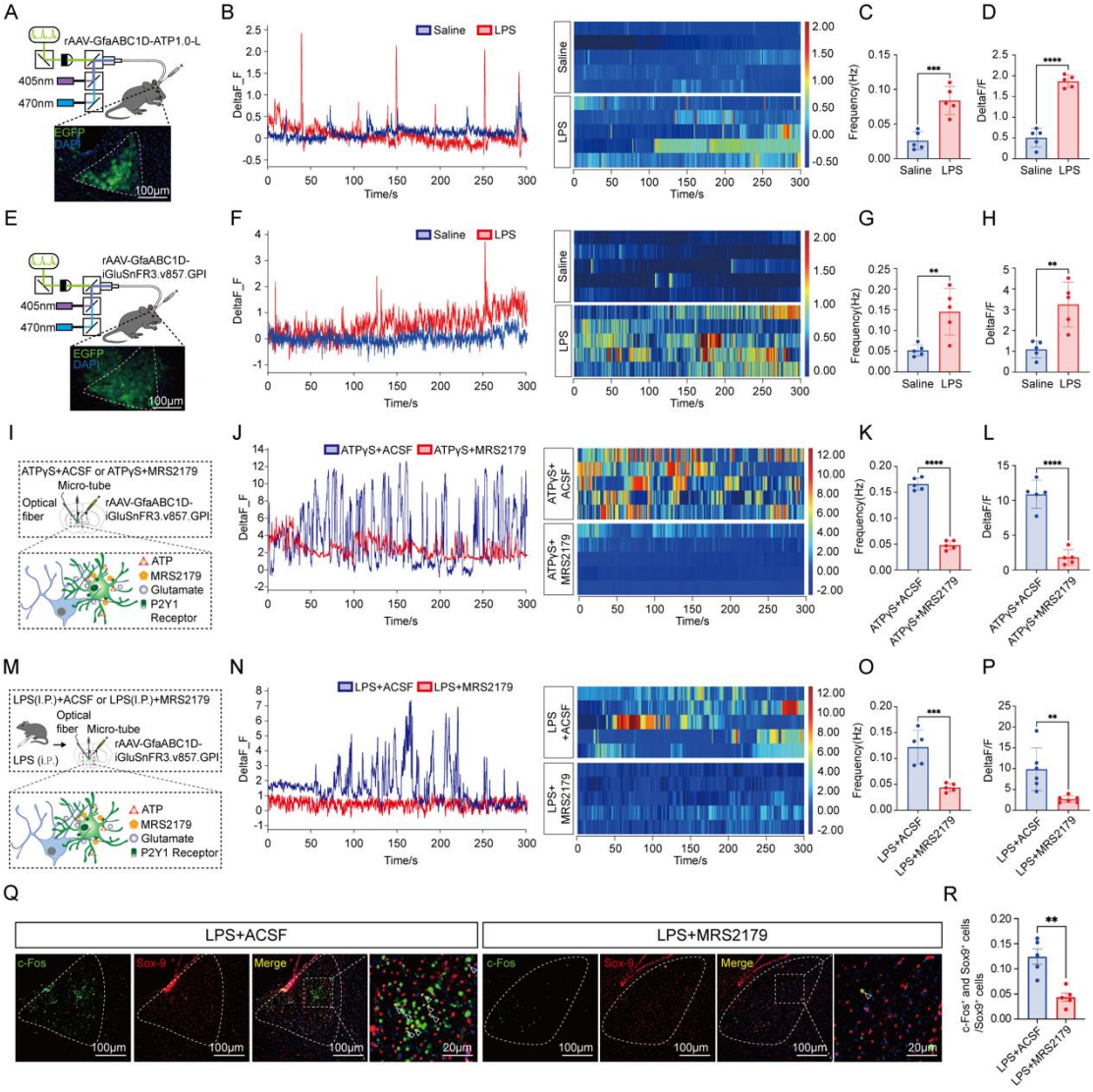


Figure 8. ATP-P2Y$_1$ Receptor Pathway Mediates Glutamate Release from Astrocytes in the dBNST

(A) Schematic of the experimental setup for detecting ATP levels around dBNST astrocytes. (B–D) Representative raw traces (B, left), heatmaps (B, right), and bar

graphs (C, D) showing ATP concentrations around dBNST astrocytes after intraperitoneal injection of LPS or saline (n=5; two-tailed t-test). (E) Schematic of the experimental setup for detecting glutamate levels around dBNST astrocytes. (F–H) Representative raw traces (F, left), heatmaps (F, right), and bar graphs (G, H) showing glutamate concentrations around dBNST astrocytes after intraperitoneal injection of LPS or saline (n=5; two-tailed t-test). (I) Schematic of the experimental setup for detecting glutamate levels around dBNST astrocytes. After local injection of a glutamate probe into the dBNST, a drug delivery cannula was implanted vertically, and an optical fiber was implanted at an oblique angle. (J–L) Representative raw traces (J, left), heatmaps (J, right), and bar graphs (K, L) showing glutamate concentrations around dBNST astrocytes after intracranial cannula infusion of ATPγS+ACSF or ATPγS+MRS2179 (n=5; two-tailed t-test). (M) Schematic of the experimental setup for detecting glutamate levels around dBNST astrocytes. After local injection of a glutamate probe into the dBNST, a drug delivery cannula was implanted vertically, and an optical fiber was implanted at an oblique angle. Mice received intraperitoneal injection of LPS together with intracranial cannula infusion of ACSF or MRS2179. (N–P) Representative raw traces (N, left), heatmaps (N, right), and bar graphs (O, P) showing glutamate concentrations around dBNST astrocytes after intraperitoneal injection of LPS and intracranial cannula infusion of ACSF or MRS2179 (n=5; two-tailed t-test). (Q) Representative c-Fos immunofluorescence images of the ACSF

group and the MRS2179 group. (R) Compared with the control group, MRS2179 reduced c-Fos expression (n=5; two-tailed t-test).

Figure 9

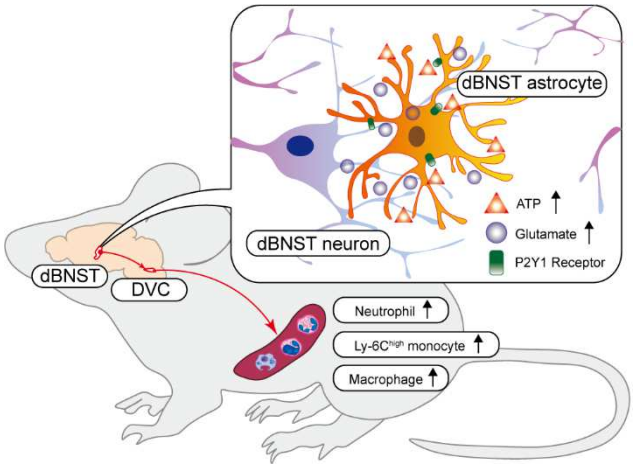


Figure 9. Schematic diagram illustrating astrocyte-neuron communication in the dBNST and the DVC-spleen axis.

LPS stimulation elevates local ATP levels in the dBNST. The increased ATP acts on astrocytic $P2Y_1$ receptors, promoting glutamate release from astrocytes. The released glutamate enhances the excitability of adjacent dBNST neurons. Fos^{dBNST} neurons partially project to the DVC, which innervates the spleen, resulting in increased splenic nerve firing, altered peripheral immune cell populations (neutrophils, Ly-$6C^{high}$ monocytes, and macrophages), and elevated pro-inflammatory cytokines (IL-1β and TNF-α).

Supplementary Files

This is a list of supplementary files associated with this preprint. Click to download.

- InflammationAssociatedNeuronalandAstrocyticEnsemblesintheDorsalBedNucleusoftheStriaTerminalisModulatePeripheralImmuneResponseviatheBrainS